

Article

Analytical, Numerical and Experimental Analysis of a Positive Displacement Cam Mechanism—A Case Study

Eugen Merticaru ¹, Vasile Merticaru ^{2,*} , Gheorghe Nagiț ² , Andrei Marius Mihalache ² ,
Liviu Lucian Tăbăcaru ² and Marius Ionuț Rîpanu ²

¹ Department of Mechanical Engineering, Mechatronics and Robotics, Gheorghe Asachi Technical University of Iasi, 700050 Iasi, Romania; eugen.merticaru@academic.tuiasi.ro

² Department of Machine Manufacturing Technology, Gheorghe Asachi Technical University of Iasi, 700050 Iasi, Romania; nagit@tcm.tuiasi.ro (G.N.); andrei.mihalache@tuiasi.ro (A.M.M.); liviu-lucian.tabacaru@academic.tuiasi.ro (L.L.T.); marius.ripanu@tuiasi.ro (M.I.R.)

* Correspondence: vasile.merticaru@academic.tuiasi.ro; Tel.: +40-723940041

Abstract: Cam mechanisms, covering a large structural variety, are widely used in machinery, mainly as components of automated systems. Their functioning behavior is affected by negative dynamic phenomena determined by specific high velocities and acceleration rates. Within the various types of research on the dynamic behavior of cam mechanisms, this study addresses the need to clarify the influence of geometrical parameters and technological conditions on some indicators of the jump phenomenon in contact loss for a cam-follower mechanism. This particularly developed case study referred to a mechanism with a profiled grooved disk cam and oscillating follower. To highlight the influence of the cam-follower contact elasticity on the jump phenomenon, two dynamic models were developed: one considering rigid elements in contact and the second considering elastic cam-follower contact. The models were tested within a virtually simulated experiment, and the numerical simulation results evidenced the influence of input factors like the applied load on the mechanism, the clearance in the cam-follower kinematic pair, and the rotational speed of the cam, and the inertia moment was reduced to the follower on some indicators of the jump phenomenon. Validation FEA and experiments were performed, proving the reliable appropriateness of the dynamic model based on elastic cam-follower contact.

Keywords: cam mechanism; dynamic behavior; influence factors; numerical modeling and simulation; experimental research; empirical mathematical models



Citation: Merticaru, E.; Merticaru, V.; Nagiț, G.; Mihalache, A.M.; Tăbăcaru, L.L.; Rîpanu, M.I. Analytical, Numerical and Experimental Analysis of a Positive Displacement Cam Mechanism—A Case Study. *Machines* **2023**, *11*, 770. <https://doi.org/10.3390/machines11070770>

Academic Editors: Hermes Giberti and Fugui Xie

Received: 29 May 2023

Revised: 18 July 2023

Accepted: 20 July 2023

Published: 24 July 2023



Copyright: © 2023 by the authors. Licensee MDPI, Basel, Switzerland. This article is an open access article distributed under the terms and conditions of the Creative Commons Attribution (CC BY) license (<https://creativecommons.org/licenses/by/4.0/>).

1. Introduction

Higher kinematic pair mechanisms, like cam mechanisms, gears, Geneva driving mechanisms (Maltese cross mechanisms), the ratchet mechanism, etc., are generally the most used in machinery and have the advantage of a superior and irreversible transmission and coupling resulting in a contact point or line but never a surface [1]. In the sense of their optimal design for higher working efficiency in conditions of avoiding vibrations, noises, shocks, or interruptions, the dynamic phenomena must be mastered. More generally, for any kind of mechanism in machinery driving chains, a reliable prediction of the dynamic behavior working through parameters like speed, acceleration, force distributions, loss coefficient, dynamic coefficient, or motion transmission function is essential in machine design. Dynamic models, analyses, and research approaches are known regarding various kinds of mechanisms, starting from a crank piston mechanism [2] or an oscillatory slider mechanism [3] up to classical distribution mechanisms [4], and ending with bionic robotic structural mechanisms [5] or complex gear transmissions [6].

Particularly for the cam mechanisms, which cover a large structural variety that are widely used in machinery, mainly as components of automated systems, the problem of negative dynamic phenomena appears in the presence of high inertial loads determined

by the specific high velocity and acceleration rates [7]. Particular operation of the cam mechanisms, as subsystems of machinery equipment like combustion engines, machine tools, packaging machines, textile machines, precision mechanical equipment, or medical devices [8], is ruled by specific sets of dynamic variables depending on geometrical parameters and technological conditions. However, all the cam mechanisms have sufficient elasticity in their components to create conditions for residual vibrations in operation [9]. Mastering the involved complex sets of structural and process variables in the sense of identification, inventory, classification, and quantification of influence factors in direct relation to operational performance parameters and further optimal adjusting of operating conditions is vital for predicting the dynamic behavior of cam mechanisms.

A synthesis review on the current state of the research field of cam mechanism dynamics highlighted several researched aspects [10], which one may group as follows:

- Research on a unified methodology for calculating the geometrical parameters and the profile curves for cams;
- Optimization of basic geometrical parameters of cam mechanisms;
- Research on quality criteria for the cam mechanisms in operation;
- Definition of new motion laws for dynamic optimization;
- Conditions determining the contact loss in cam mechanism coupling;
- Loads and forces in cam mechanism operation. Problems in camshaft torsion minimization;
- Shocks and vibrations in cam mechanism operation;
- Dynamic models for cam mechanism research;
- Dynamic comparison of cam mechanism structure;
- Influence of the clearance in kinematic pair on the dynamic behavior;
- Influence of the accuracy and the wear on the cam profile and the operating vibrations on the precision of the follower motion in cam-follower mechanisms.

The following types of cam mechanisms were studied concerning the methodologies for calculating the geometrical parameters and the profile curves for the cams: plane mechanisms with disk cams having external profiles or profiled grooves, with oscillating or translating followers, those having rollers or being flat-faced, and also spatial mechanisms with cylindrical cams. Tiboni et al. [11] proposed the use of an evolutionary algorithm for the representation of the movement, and, therefore, of the cam profile, based on the modified trapezoidal motion law, also known as the modified seven segments. Faxin and Xianzhang [12] presented a software solution developed on the VB (Visual Basic language) platform for designing the moving tracks and the cam's profile in the case of a parallel combination of cam mechanisms.

Research studies on the optimization of basic geometrical parameters of cam mechanisms mainly approached mechanisms with disk cams and oscillating or translating followers and rollers and targeted the minimization of the cam's dimensions and wear, imposing restrictions related to the pressure angle, the curvature radius for the cam and the follower roller, the contact stress in the coupling cam-follower, the mechanism's overall dimensions, or the radius of tool for machining the cam profile. Mohan Kumar et al. [13] proposed an algorithm and a software tool for designing some disk cams for single spindle automats under the limitations of the pressure angle and curvature radius. Petrescu [14] proposed a method of geometric synthesis for the cam mechanism and translated the tappet with a roll that used only the geometric parameters without considering the velocities and utilizing a condition to realize the tappet the velocities imposed by the motion laws. Kim et al. [15] developed a study on the optimal synthesis of a spring-actuated cam mechanism using a cubic spline, which was able to satisfy asymmetric constraints and guarantee continuous contact at the cam-follower interface. Based on a dynamic model built for a complete spring-actuated cam system, the optimized cam was compared with a cam having constant angular velocity and a polynomial cam.

For the evaluation of cam mechanism operation, a set of quality criteria have been identified and inventoried [16]: the mechanic operation efficiency, the force multiplying

coefficient, the coefficient of stiffness for mechanism parts, the coefficient of friction losses in kinematic couplings, the degree of distancing the mechanism from blockage zones, and the overall dimensions of the mechanism. Naskar and Acharyya [17] conducted extended experimental research for measuring the dynamic response of jerk-optimized, stress-optimized, and size-optimized cams. The method adopted to measure the performance of the cam drive considered the elastic deformation of the cam surface due to induced stresses and established the causes behind the deviations of the theoretical cam displacements from the actual displacements.

A motion law that provides adequate dynamics of cam mechanisms has to deal with continuous time functions of the acceleration and the jerk that present the least possible values for the maximum acceleration. The quality criteria for the follower motion law would consider avoiding soft and hard shocks. Research studies in the direction of motion law optimization proposed solutions using polynomials, cubic spline curves, and finite Fourier series. Yoon and Rao [18] proposed piecewise cubic spline functions for representing the follower displacement and the minimum norm principle for the general synthesis of cam motion. Müller et al. [19] used Mechanism Developer (MechDev) as a software tool in the research on the optimization of the transmission angle and the curvature of cam mechanisms. He also applied Non-Uniform Rational B-Splines (NURBS) for modeling the angular input of a cam from a cam mechanism with a prismatic roller-follower. Nguyen [20] used the properties of NURBS for studying the motion curves for the follower of cam mechanisms, including peak values of the acceleration and jerk, and proved advantageous characteristics compared to classical approaches.

Regarding the conditions determining the contact loss in cam mechanisms coupling, the jump of the follower under high-speed rates or vibrations has been mainly studied. Sadek and Daadbin [21] approached the dynamic modeling of a torsion bar cam mechanism from a packaging machine, showing that the follower jumps appear mostly in the phase of positive acceleration, determined by the vibrations of the mechanism under high-speed operation. Research on the exact response of a follower system was performed by Bagci and Kurnool [22]. The proposed method used Laplace Transforms allowing one to determine the critical cam speeds and the possible follower jump conditions. De Groote et al. [23] used recurrent neural networks to estimate the follower jump trajectory, based on cam rotation measurements, for a wide range of operating conditions and system modifications. Their research proposed the use of an additive feature attribution method to quantify the contribution of features in a multivariate time series on the prediction output of recurrent neural network models.

Loads and forces in cam mechanism operation have been analyzed mainly for mechanisms with disk cams and translation or oscillating followers and combined cam-bar mechanisms. Camshaft torque fluctuations have been also studied, and solutions for the minimization of reactions in couplings have been proposed. Sadler and Yang [24] applied nonlinear programming techniques to the design of systems consisting of a four-bar linkage driven by a disk cam, targeting as an objective the minimization of input torque fluctuation under the assumed condition of constant input angular velocity of the cam. Hejma et al. [25] proposed a methodology for the calculation of torque according to the desired angular velocity of the cam. Particularly, a cubic polynomial, the fifth-degree polynomial, and the seventh-degree polynomial were studied. Jin et al. [26] proposed a mathematical model for a roller cam rail mechanism used as a conversion mechanism in a 2D pump for avoiding sliding friction pairs and optimizing the force balance conditions in the pump at higher operating speeds. Experiments were developed to demonstrate the model's precision and the effectiveness of the mechanism. Problems in camshaft torsion minimization were also approached by Guilan et al. [27], who proposed a solution to install a flywheel on the output shaft of an additional cam linkage mechanism to producing an opposite kinetic energy fluctuation that can counteract the effect of the energy fluctuation.

Research studies highlighted that in cam mechanism operation, a motion law with finite discontinuities of speed may determine hard shocks, and a motion law with finite

discontinuities of accelerations may determine soft shocks. Vibrations in cam mechanisms have been studied in relation to the motion law, the elasticity of the mechanism, the fluctuations of cam speed, etc. Considering oscillations of both the cam drive system and the follower, Ambardekar and Gupta [28] proposed an optional control to the cam input designed to minimize positional error in the output. The cam motion is stochastically simulated and analyzed. Hsu and Pisano [29] proposed a distributed parameter dynamic model to investigate the dynamic responses of a finger follower cam mechanism. The model considers a hydraulic lash adjuster with an oscillating pivot, and also the frictional forces between the sliding surfaces. Liu [30] applied Finite Element Analysis (FEA) for an elastic slider crank follower linkage, considering the elastic deflections induced by the large inertia of the linkage operating at a fluctuating high speed of the driving cam.

Together with those methods presented above, several other dynamic models for cam mechanisms research can be nominated. Dresner and Barkan [31] performed a brief review of the literature on the dynamic analysis of flexible cam-follower systems, highlighting the following goals: predict when and if the follower jumps off the cam, determine the cam contact forces and the linkage forces, establish the closing spring requirements, determine the magnitude of any follower impact with its seat, and help optimize the system's dynamic response. They also recommended a method for the analysis of such systems and an extension of this analysis method to multi-input systems. Wang [32] proposed a model based on FEM (Finite Element Method) in time for the vibrating elastic mechanisms with clearances, where the periodic response is described in terms of a set of temporal nodes of all spatial degrees of freedom in the system. The model is applied in the study of a cam-driven valve train. Paradorn [33] developed a three-mass, two-DOF (degrees of freedom) dynamic model for the simulation of a controlled impact and over-travel cam-follower mechanism, specific to automatic assembly machines. A two-step mesh stiffness model for the active and dwell periods, a torque compensation cam (TCC), and a torque compensation flywheel (TCF) was proposed by Kuang et al. [34] to investigate the correlation between the dynamic response of a globoid cam (GC) system and the motor driving speed. Desai and Patel [35] used Excel sheets to perform a complete kinematic and dynamic analysis of the cam and follower mechanisms, and critical angular speed was determined for each design to predict when the follower jumps off the cam. The analytical method was used, and the dynamic force analysis determined the cam contact forces and values of kinematic parameters at which the design fails. Zhang et al. [36] performed a dynamic simulation for a cam-follower mechanism on a model developed using ADAMS software using a virtual prototype built in Pro/E. MSC ADAMS software was also used within a dynamic analysis on a virtual model for a cam-follower mechanism by Delyová et al. [37], who proposed the method of reducing weight and force value on a moving member of the mechanism in dynamic modeling. Jomartov [38] used SimulationX software environment to develop a multi-body dynamic model for the Russian Sulzer loom STB considering the transition processes, the backlash at the joints and nodes, the force of resistance, and the electric motor performance. Based on the principle of equivalent substitution of components, Deng et al. [39] proposed a dynamic virtual model for the cam linkage mechanism from the push device of a chocolate packaging machine. The dynamic analysis within MATLAB/Simulink software, considering the elastic deformation of the member, highlighted an important effect of the lateral deformation of the camshaft on the cam motion. Jiang et al. [40] modeled the relationship between the cam profile and the actuation trajectory and applied the cubic spline interpolation method in the cam profile generation; the study approached the case of a gravity-driven tricycle.

A dynamic comparison of the cam mechanism's structure was researched by Vo and Le [41]. They analyzed the dynamic response of an innovative quasi-zero stiffness pneumatic vibration isolator (QZSPVI) using two mechanisms, including a wedge and a semicircle cam. The results of the study highlighted the advantages of the proposed model against the equivalent pneumatic vibration isolator (EPVI), which had only the wedge mechanism in its structure.

The influence of the clearance in kinematic couplings on the dynamic behavior of cam mechanisms has been studied by several research investigations. Osman et al. [42] analyzed the dynamic behavior under vibrations for a mechanism with a disk cam and a translating follower by considering the clearances in the rotation coupling of the cam and the rotation coupling roller follower in comparison with the situation of neglecting the clearances. The results proved important modifications for the accelerations, the reaction forces, and the torque on the camshaft. Wang [32] analyzed the influence of the clearances from a distribution mechanism with a cam and a translating flat-faced follower and showed that the clearance between the valve and its seat determines impact between the valve and its seat, loss in the follower-cam contact, and impact between the follower and the cam. Chang et al. [43] proposed a new fault diagnosis method in relation to the clearance and recoil of the cylinder cam mechanism. The method is based on the Variational Box Dimension Kernel Fuzzy Mean Clustering Algorithm (VK algorithm), which combines the variational mode decomposition and fractal box-counting dimension (VMD-FBCD), and the fuzzy clustering algorithms were determined with a kernelized Mahalanobis distance (KMD-FC).

The precision of the follower motion in cam-follower mechanisms was also studied in relation to the influence of the accuracy and of the wear on the cam profile and the operating vibrations. Rao [44] defined the flexibility error as the difference between the desired output motion and the real one for the follower, which was determined by the inertia and the elasticity of the mechanism. His research separated the flexibility error from the mechanical and structural errors and proposed a method to calculate the elasticity of the contact spring or the mechanism for the minimization of flexibility error. Lassaad et al. [45] investigated the nonlinear dynamic behavior and the influence of the cam profile error on it for a cam mechanism with an oscillating roller follower. The analysis is based on a nonlinear lumped-mass model including eight degrees of freedom with two nonlinear Hertzian contacts. The model was described by second-order differential equations, which were solved by using the implicit Newmark algorithm combined with the Newton–Raphson iterative scheme. De Groote et al. [46] presented a hybrid model architecture consisting of a close interconnection of neural and physics-based network layers, which can accurately simulate the system behavior and estimate the set of critical system parameters that lead to hazardous jump phenomena in cam-follower systems. Lin et al. [47] considered the machine undercutting, the roller limit load, and the contact stresses within a dynamic analysis of a compact cam reducer, which can be used as a rigid drive mechanism, proposing an optimal design through adjustment of the cam size, turret dimension, eccentricity, and roller size. Flocker [48] proposed and studied a modified trapezoidal cam profile with an adjustable forward and backward acceleration, suitable for the single-dwell cam and follower applications. Follower acceleration determining the interface forces was discussed as one of the primary factors affecting the cam wear and the follower jump phenomena.

By analyzing the above considerations on the current state in the research field, the need for extended research on the dynamic behavior of cam mechanisms with bilateral higher kinematic pairs, and oscillating followers when considering the shocks resulted in contact loss and contact restoration, and the influence of cam equilibration or the influence of generalized mass, was highlighted as a current problem.

Within the various types of research on the dynamic behavior of cam mechanisms, the purpose of this study is to address the need to clarify the influence of geometrical parameters and technological conditions on some indicators of the jump phenomenon in contact loss for a cam-follower mechanism.

The research purpose derived a set of particular objectives as follows: the development of reliable dynamic models for the studied type of mechanism, testing and validation of the models through numerical simulation using customized developed software tools, FEA analysis on the coupling contact, and experimental testing and validation.

2. Materials and Methods

The particularly developed research referred to a mechanism with a profiled grooved disk cam and oscillating follower with a roller, which represented a sub-assembly of an automated feeding system from a textile machine and, more precisely, a part of the driving kinematic chain of the yarn catcher from a weaving loom machine type STB-216 (Russian product under Sulzer licence). Several types of cam mechanisms are included in the automation structure of such loom machines [38,49].

The kinematic diagram of such a mechanism is shown in Figure 1a, where the kinematic elements of the mechanism are as follows: 1 is the cam, 2 is the follower, 3 is the follower roller, 4 is a slider (the yarn catcher), 5 is a slide block, and 6 is the fixed element (frame). The other symbols in Figure 1a represent A, B, C, D, E, F, G, H, and N, which are the characteristic points in the geometrical calculation diagram, f_i is the angular position of the kinematic element i , ω_i is the angular velocity of kinematic element i , ψ_0 is the minimum angle for the follower, and ψ is the angular displacement of the follower. Figure 1b shows some additional geometrical elements used in calculating the developed dynamic models, and K_i is the mass center for the kinematic elements i and θ_{i0} is the angular position of the mass center for the kinematic element i .

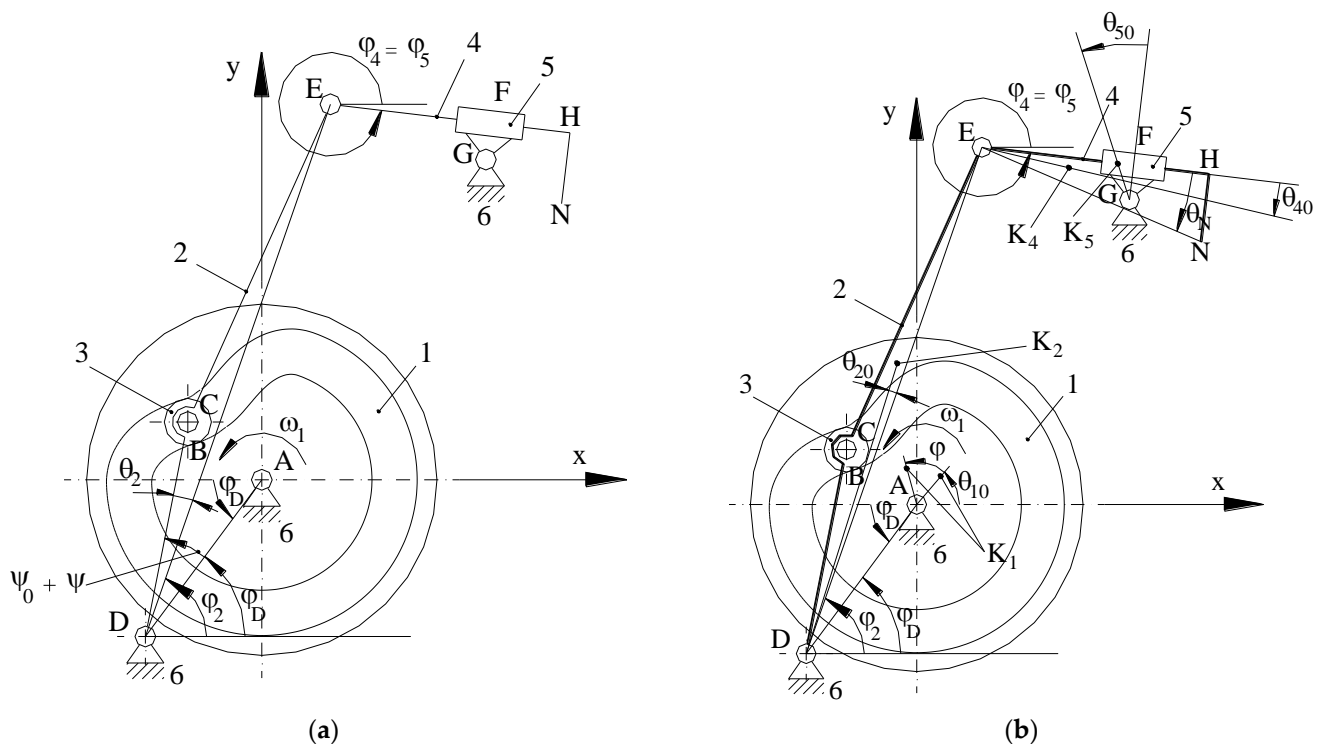


Figure 1. The studied mechanism with a disk cam and oscillating follower: (a) kinematic diagram of the mechanism [42]; (b) geometric calculation diagram in modeling.

The particular values for the dimensional parameters of the mechanism presented in Figure 1 are as follows: the diameter of the disk cam is $D = 120$ mm, the distance between the axis of the cam and the axis of the oscillating follower is $AD = d = 69$ mm, the length of the oscillating follower is $DC = l = 61$ mm, the follower roller radius is $R = 8$ mm, the length of the kinematic element 4 is $EH = 215.5$ mm, the positional distances are $DE = 186$ mm, $FG = 13.75$ mm, and $AG = 132$ mm, and the positional coordinates are $x_D = -34.07$ mm, $y_D = -60$ mm, $x_G = 71.5$ mm, and $y_G = 110.9$ mm. We also mention that the minimum value of the real profile on the cam groove is $r_{r \min} = 24$ mm and the maximum value of the real profile on the cam groove is $r_{r \max} = 40.428$ mm. Furthermore, the rotation speed for the cam is in the range $n = 180 \div 240$ rev/min, which means that the angular velocity for the cam, $\omega_1 = \frac{\pi \cdot n}{30}$, is in the range $\omega = 18.85 \div 25.13$ rad/s.

2.1. Dynamic Models

The influence of the cam-follower contact elasticity on the jump phenomenon was researched based on the idea to develop two dynamic models: one considering rigid elements in contact and the second considering elastic cam-follower contact [50].

2.1.1. Dynamic Model with Rigid Elements

The first proposed dynamic model with rigid elements was developed as a reducing element model with the cam being chosen as a reducing element in the case of operation without jump (the backlash in the pair cam-follower would be $j = 0$).

- Theoretical conditions in modeling considered a set of simplifying hypotheses based on the following assumptions:
- The masses and the inertia moments of the kinematic elements of the driving chain from the electrical motor up to the camshaft were neglected;
- The friction in kinematic couplings was neglected;
- The rotational kinetic energy for the follower roller was neglected;
- If backlash j is nonzero, the jump of the follower occurs when the reaction force R_{13} between the cam and the follower becomes equal to zero or it changes its sign;
- During the follower's jump, the cam and the motor move together, and independently of them, the follower moves together with the kinematic elements linked to it;
- The impact between the cam and follower that occurs when the follower comes in contact with one of the flanks of the profiled groove of the cam was considered perfectly elastic and instantaneous.

For the jump period, the dynamic model of the mechanism has 2 DOF (degrees of freedom). The motor and the cam were modeled by a dynamic model-reducing element, with the cam considered as the reducing element. The dynamic model-reducing element for the follower with the elements linked to it considered the follower as the reducing element.

Under such circumstances, the differential equation of motion for $j = 0$ was written as follows:

$$J_{red} \times \frac{d\omega_1}{d\varphi_1} \times \omega_1 + \frac{\omega_1^2}{2} \times \frac{dJ_{red}}{d\varphi_1} = M_{red}^m + M_{red}^r \quad (1)$$

where:

$$J_{red}(\varphi_1) = \sum_{i=1, i \neq 3}^5 \left[m_i \times \left(\frac{v_{Ki}}{\omega_1} \right)^2 + J_i \times \left(\frac{\omega_i}{\omega_1} \right)^2 \right] + \left[m_3 \times \left(\frac{v_C}{\omega_1} \right)^2 \right] + \left[J_m \times \left(\frac{\omega_m}{\omega_1} \right)^2 \right] \quad (2)$$

$$M_{red}^m(\omega_1) = \bar{M}_1 \times \frac{\omega_1}{\omega_1}$$

$$M_{red}^r(\varphi_1, \omega_1) = \sum_{i=1}^5 \left(\bar{G}_i \times \frac{\bar{v}_{Ki}}{\omega_1} \right) + \left(\bar{F}_u \times \frac{\bar{v}_N}{\omega_1} \right)$$

The physical quantities that appear in Equations (1) and (2) are as follows: J_{red} is the inertia moment reduced to the cam, v_{Ki} is the velocity of the mass center of the kinematic element i , v_C is the velocity of the mass center of the follower roller, ω_i is the angular velocity of the kinematic element i , ω_m is the angular velocity of the motor, m_i is the mass of the kinematic element i , J_i is the inertia moment of the kinematic element i defined related to an axis perpendicular to the plane of motion and passing through the mass center of the element i , M_{red}^m is the driving moment reduced to the cam, M_{red}^r is the resistant moment reduced to the cam, G_i is the gravity force of the kinematic element i , F_u is the load acting on the kinematic element 4, v_N is the velocity of point N where the force F_u was applied, and M_1 is the driving moment acting on the camshaft, given by Equation (3).

$$M_1(\omega_1) = i_t \times \frac{M_n \times (\omega_1 \times i_t - \omega_s)}{(\omega_n - \omega_s)} \quad (3)$$

In Equation (3), i_t is the transmission ratio from the motor to the camshaft, M_n is the nominal moment of the motor, ω_n is the nominal angular velocity of the motor, and ω_s is

the synchronism angular velocity of the motor. Equation (3) was derived considering the linear portion of the stable operation, under load, of the characteristic of the three-phase asynchronous motor.

For the jump period, the differential equation of motion for the cam became:

$$J'_{red} \times \frac{d\omega_1}{d\varphi_1} \times \omega_1 + \frac{\omega_1^2}{2} \times \frac{dJ'_{red}}{d\varphi_1} = M_{red}^m + M'_{red} \tag{4}$$

where:

$$J'_{red}(\varphi_1) = m_1 \times \left(\frac{v_{K1}}{\omega_1}\right)^2 + J_1 \times \left(\frac{\omega_1}{\omega_1}\right)^2 + J_m \times \left(\frac{\omega_m}{\omega_1}\right)^2 M'_{red}(\varphi_1, \omega_1) = \bar{G}_1 \times \frac{\bar{v}_{K1}}{\omega_1}, \tag{5}$$

and M^m_{red} is given by Equation (2). Similarly, for the follower, during the jump:

$$J''_{red} \times \frac{d\omega_2}{d\varphi_2} \times \omega_2 + \frac{\omega_2^2}{2} \times \frac{dJ''_{red}}{d\varphi_2} = M''_{red} \tag{6}$$

where:

$$J''_{red}(\varphi_2) = \sum_{i=2, i \neq 3}^5 \left[m_i \times \left(\frac{v_{Ki}}{\omega_2}\right)^2 + J_i \times \left(\frac{\omega_i}{\omega_2}\right)^2 \right] + \left[m_3 \times \left(\frac{v_C}{\omega_2}\right)^2 \right] \tag{7}$$

$$M''_{red}(\varphi_2, \omega_2) = \sum_{i=2}^5 \left(\bar{G}_i \times \frac{\bar{v}_{Ki}}{\omega_2} \right) + \left(\bar{F}_u \times \frac{\bar{v}_N}{\omega_2} \right)$$

The velocity of the cam and the follower, immediately after the impact, were determined using the Lagrange equations for the impulsive motion of a system with 2 DOF and the equation from Newton’s hypothesis. So, for the dynamic model of the cam:

$$J'_{red} \times \omega_1 - J'_{red} \times \omega_1^0 = \bar{M}_A(\bar{P}_{int1}) \times \frac{\bar{\omega}_1}{\omega_1} \tag{8}$$

and for the dynamic model of the follower:

$$J''_{red} \times \omega_2 - J''_{red} \times \omega_2^0 = \bar{M}_D(\bar{P}_{int2}) \times \frac{\bar{\omega}_2 v_{C12n}}{\omega_2 v^0_{C12n}} = -k \tag{9}$$

where J'_{red} , J''_{red} are given by Equations (4) and (6), respectively, ω_1^0 , ω_1 are the angular velocities of the cam before and immediately after the impact, respectively, ω_2^0 , ω_2 are the angular velocities of the follower before and immediately after the impact, respectively, \bar{P}_{int1} and \bar{P}_{int2} are the interior percussions acting on the cam, and on the follower in the cam-follower contact point, $\bar{M}_A(\bar{P}_{int1})$ and $\bar{M}_D(\bar{P}_{int2})$ are the moments of percussions, \bar{P}_{int1} and \bar{P}_{int2} , with respect to points A and D (see Figure 1), v^0_{C12n} and v_{C12n} are the relative velocities of point C from the follower (C_2) with respect to point C from the cam (C_1) before and after the impact, which are projected on the common normal direction at the cam profile, and k is the coefficient of restitution (impact elasticity). For perfectly elastic impact, $k = 1$.

The angular velocities of the cam, the follower after impact, and the interior percussions \bar{P}_{int1} or \bar{P}_{int2} resulted in the following equation:

$$\omega_2 = \frac{J'_{red} \times \omega_1^0 \times A1 \times A2 \times (1+k) + \omega_2^0 \times [J''_{red} \times (A1)^2 - J'_{red} \times (A2)^2 \times k]}{J'_{red} \times (A2)^2 + J''_{red} \times (A1)^2} \tag{10}$$

$$\omega_1 = \frac{\omega_2 \times A2 + \omega_2^0 \times A2 \times k - \omega_1^0 \times A1 \times k}{A1}$$

$$P_{int1} = \frac{J''_{red} \times \omega_2 - J'_{red} \times \omega_2^0}{-A2}$$

where the notations $A1$ and $A2$ represent the following equations:

$$\begin{aligned} A1 &= AC_x \times \sin\left(\varphi_2 + \theta_2 + \alpha + \frac{\pi}{2}\right) - AC_y \times \cos\left(\varphi_2 + \theta_2 + \alpha + \frac{\pi}{2}\right) \\ A2 &= DC_x \times \sin\left(\varphi_2 + \theta_2 + \alpha + \frac{\pi}{2}\right) - DC_y \times \cos\left(\varphi_2 + \theta_2 + \alpha + \frac{\pi}{2}\right) \end{aligned} \quad (11)$$

The dynamic model involved systems of nonlinear second-order differential equations with variable coefficients. The mathematical solving required numerical integration, and the Newton–Raphson method was applied.

2.1.2. Dynamic Model with Elastic Contact

The second proposed dynamic model with elastic contact was developed as a dynamic model with 1 DOF (degree of freedom), as presented in Figure 2.

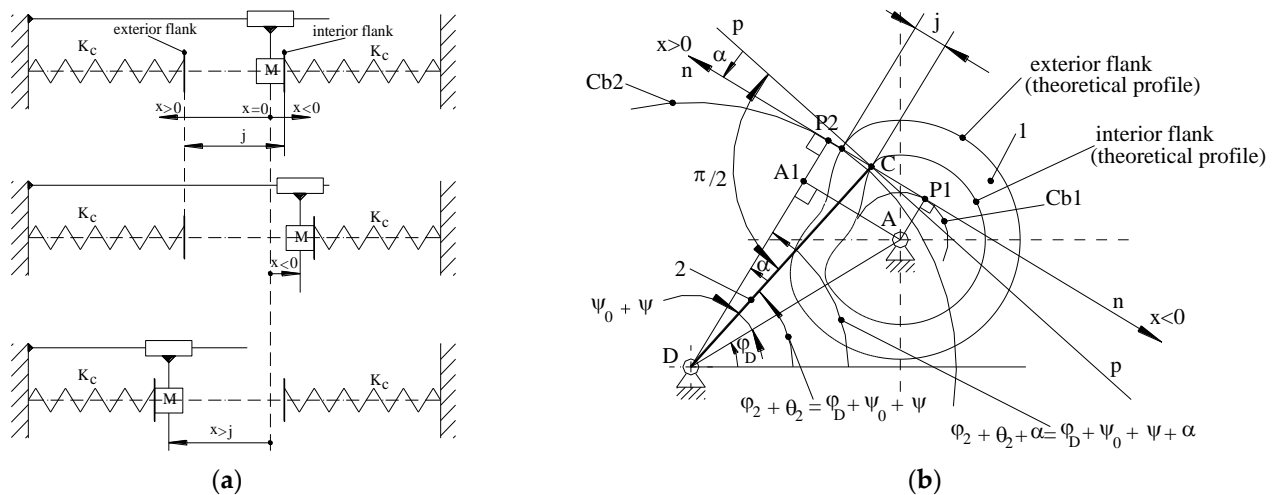


Figure 2. The dynamic model with 1 DOF and with elastic contact: (a) the model symbolized representation; (b) calculation of the geometric diagram.

Theoretical conditions in modeling considered a set of simplifying hypotheses based on the following assumptions:

- Only the elasticity of the contact cam-follower was considered, and the other elements of the mechanism were considered rigid;
- A relative motion occurs between the cam and the follower along the common normal direction at the contact point;
- As a criterion to detect the jump of the follower, the relative displacement cam-follower was used. When the relative displacement becomes equal to zero or changes the sign, the jump occurs.

In Figure 2a, the symbols are as follows: M is the reduced mass of the mechanism (kg); j is the backlash in the higher pair cam-follower (mm); x is the relative displacement cam-follower along the common normal direction at the contact point (mm); and K_c is the rigidity of the contact cam-follower (N/mm). The origin of the x -axis was chosen in the contact point C of the follower with the interior flank of the cam (see Figure 2b). The positive sense of the x -axis was chosen for the exterior of the cam, and the negative sense was for the interior of the cam. The other symbols in Figure 2b are shown according to those in Figure 1.

The differential equations for the relative motion cam-follower were written as follows: For contact with the interior flank ($x \leq 0$):

$$M \times \ddot{x} + K_c \times x^n = R_{31} \ddot{x} = \frac{d^2x}{dt^2}; \quad n = \frac{10}{9} \quad (12)$$

For the follower jump ($0 < x < j$):

$$M \times \ddot{x} = R_{31} \quad (13)$$

For contact with the exterior flank ($x \geq j$):

$$M \times \ddot{x} + K_c \times (x - j)^n = R_{31} \quad (14)$$

In Equations (12)–(14), the other parameters are as follows: R_{31} is the static reaction of the cam on the follower (neglecting friction), t is the time (s), and n is an exponent corresponding to the elastic force of contact F_{elc} (N), which was the calculated function of the contact deformation x , as shown below [51]:

$$F_{elc} = K_c \times x^n K_c = 8.05 \times 10^4 \times (l_w)^{\frac{8}{9}} \quad (15)$$

where l_w is the length of the contact between the cam and the follower roller (mm).

Also, in Equations (12)–(14), M is the reduced mass of the mechanism, which is given by:

$$M = \frac{M_1 \times M_2}{M_1 + M_2} \quad M_1 = \frac{4 \times J_{cam}}{D_{b1}^2}; \quad M_2 = \frac{4 \times J_{follower}}{D_{b2}^2} \quad (16)$$

where M_1 is the reduced mass of the cam (kg), M_2 is the reduced mass of the follower (kg), and J_{cam} and $J_{follower}$ are the inertia moments for the cam and the follower, which are given by the following formulas:

$$J_{cam} = J_{r1} + J_{rm} J_{follower} = J_{r2} + J_{r4} + J_{r5} + J_{r3} J_{r3} = m_3 \times \left(\frac{v_c}{\omega_2} \right)^2 \quad (17)$$

where J_{r1} is the moment of inertia of the cam reduced to the cam, J_{rm} is the moment of inertia of the motor reduced to the cam, J_{r2} is the moment of inertia of the follower reduced to the follower, J_{r4} is the moment of inertia of kinematic element 4 reduced to the follower, J_{r5} is the moment of inertia of kinematic element 5 reduced to the follower, and J_{r3} is the moment of inertia of the follower roller reduced to the follower.

Also, in Equation (16), D_{b1} is the diameter of the circle with the center in A, which is tangent to the common normal $n-n$ (see Figure 2b), and D_{b2} is the diameter of the circle with the center in D, which is tangent to $n-n$ (see Figure 2b) and is given by:

$$D_{b1} = 2 \times |l \times \cos \alpha - d \times \cos(\psi_0 + \psi + \alpha)| \quad D_{b2} = 2 \times l \times \cos \alpha \quad (18)$$

where l is the length DC of the follower, d is the distance between the cam axis and the follower axis AD (see Figure 2b), and α is the pressure angle of the mechanism.

Once the relative displacement cam-follower x was calculated, the position angle φ_{2nel} and the angular velocity ω_{2nel} for the follower could be calculated from the motion law of the cam, with the formulas:

$$\varphi_{2el} = \varphi_{2nel} + \frac{x}{l \times \cos(\alpha)} \omega_{2el} = \omega_{2nel} + \frac{\dot{x}}{l \times \cos(\alpha)} \quad (19)$$

2.2. Numerical Models Solving and Simulated Experiment Conditions

Numerical integration of the motion equations corresponding to the above-presented dynamic models, together with numerical simulation for virtually testing the models, were performed using a customized engineering software package developed by modular, procedural programming under a MATLAB® environment.

The input numerical data in the numerical calculation were, in relation to Figures 1 and 2, as follows: $l = CD = 61 \times 10^{-3}$ (m), $DE = 186 \times 10^{-3}$ (m), $FG = 13.75 \times 10^{-3}$ (m), $x_G = 72 \times 10^{-3}$ (m), $y_G = 111 \times 10^{-3}$ (m), $x_D = -34.073 \times 10^{-3}$ (m), $y_D = -60 \times 10^{-3}$ (m), $\varphi_D = 60.408^\circ$,

$\psi_a = 15^\circ$, $\psi_o = 27.627^\circ$, $\varphi_u = 58^\circ$, $m_1 = 2.6271$ (kg), $J_1 = 2278.84 \times 10^{-6}$ (kg·m²), $m_2 = 0.3681$ (kg), $J_2 = 1161.71 \times 10^{-6}$ (kg·m²), $m_3 = 0.0075$ (kg), $m_4 = 0.1266$ (kg), $J_4 = 905.444 \times 10^{-6}$ (kg·m²), $m_5 = 0.0474$ (kg), $J_5 = 9.2201 \times 10^{-6}$ (kg·m²), $J_m = 0.007$ (kg·m²), $AK_1 = 0.6796 \times 10^{-3}$ (m), $DK_2 = 76.4865 \times 10^{-3}$ (m), $EK_4 = 155.859 \times 10^{-3}$ (m), $\theta_{40} = -2.087129^\circ$, $GK_5 = 9.8297 \times 10^{-3}$ (m), $\theta_{10} = 181.939487^\circ$, $\theta_{20} = 1.408967^\circ$, $\theta_{50} = 0^\circ$, $EN = 265.0226 \times 10^{-3}$ (m), and $\theta_N = -9.995456134^\circ$. The workload F_u acting on kinematic element 4 in point N (see Figure 1) was considered to have the components $F_{ux} = F_u$ and $F_{uy} = 0$, opposing at any moment to the relative translating motion of kinematic element 4 in relation to kinematic element 5. A 3-phase asynchronous electric motor with a nominal power of $P_n = 1.1$ (kW), a synchronism rotation speed of $n_{sm} = 1000$ (rpm), and a nominal rotation speed of $n_m = 920$ (rpm) was considered in the calculation.

For virtually testing the developed models and highlighting the influences of the geometrical parameters and the technological conditions on the dynamic behavior of the studied mechanism, numerical simulations were performed within a simulated experiment, which were organized on a 2⁴ plan.

As influence factors, the following were considered: the applied load (load force) F_u , the backlash j in the bilateral higher kinematic pair cam-follower, the rotation speed n_1 of the cam, and the inertia moment J_t of the follower and all kinematic elements linked to it, which were reduced to the follower.

Numerical simulation studied two laws of motion: the law of motion with sine acceleration and the law of motion with cosine acceleration. The calculation was performed only for the rising phase of the follower.

Again, two different situations for the angular velocity ω_1 of the cam were studied: the ω_1 variable, resulting from integrating the motion equation of the dynamic model, and the $\omega_1 = \text{constant}$.

For the dynamic model with rigid elements, the following parameters were considered as indicators for the jump phenomenon: the moment $(M_{R13D})_{\max}$ of the cam-follower reaction, the deviation $(\varphi_{2rcj} - \varphi_{2rfj})_{\max}$ of the follower's angular position determined by the backlash, the deviation $(\omega_{2rcj} - \omega_{2rfj})_{\max}$ of the follower's angular velocity determined by the backlash, the deviation $(\omega_{1rcj} - \omega_{1rfj})_{\max}$ of the cam's angular velocity determined by the backlash, the percussion $(Percussion_{\text{int}})_{\max}$ at cam-follower impact, and the number of jumps (*Jumps no.*) for the follower on the ascending phase.

For the dynamic model with elastic contact, the following parameters were considered as indicators for the jump phenomenon: the moment $(M_{R13D})_{\max}$ of the cam-follower reaction, the relative displacement of the follower in relation to the cam $(x_{el})_{\max}$, and the number of jumps (*Jumps no.*) for the follower.

The values of the two considered levels for the input factors within the simulated experiment are shown in Table 1.

Table 1. Values for the levels of the input factors within the 2⁴ simulated experiment.

Factor Level	Factor			
	A (F_u) (N)	B (j) (mm)	C (n_1) (rpm)	D (J_t) (kg·m ²)
1	0	0.016	180	$J_t = 1 \cdot J_t$
2	65	0.128	300	$J_t = 4 \cdot J_t$

2.3. Finite Elements Analysis on the Contact in the Cam-Roller Coupling

An FEA (Finite Elements Analysis) on the contact in the coupling cam-roller was also performed for virtual testing of the dynamic models. Due to limited computing power, the CAE model was simplified to the cam and roller only since the results were based on the interaction between the two. The purpose of the FEA approach was to replicate, in the CAE (Computer-Aided Engineering) model, the relative motion inside the cam-follower assembly, with conditions similar to those considered within the theoretical research that were previously described by the dynamic models and numerically simulated under a MATLAB[®] environment. That was expected to lead in simulation to a full interaction

between the components in contact between the follower roller and the cam groove flank, and even to determine small gaps corresponding from the follower jumps of similar amplitudes to those predicted by the results of the numerical simulations. Ansys® was chosen as the FEA software tool.

For modeling the full motion of the follower roller along the imposed path on the cam profile, a 3D CAD assembly model was designed in Siemens SolidEdge®. The internal and external profile curves from the real cam (see Figure 3a) were generated using the *Curve by Table* modeling command under the *Surfacing* toolbar, as shown in Figure 3b. Each profile curve was defined by a set of points; the corresponding coordinate calculated data was imported from an MS Excel datasheet. The 3D model in Figure 3a corresponds to the cam profile with the law of motion with sine acceleration. A supplementary curve was defined in the 3D cam model to define the middle path of the roller in the assembly model and properly place the roller in the desired initial position. The cam and the follower roller were constrained in the assembly model using the *Path* option under the *Cam Design* capability, as shown in Figure 3c. The assembly CAD model was saved in *Parasolid* format to be imported as geometry data in the Ansys CAE model.

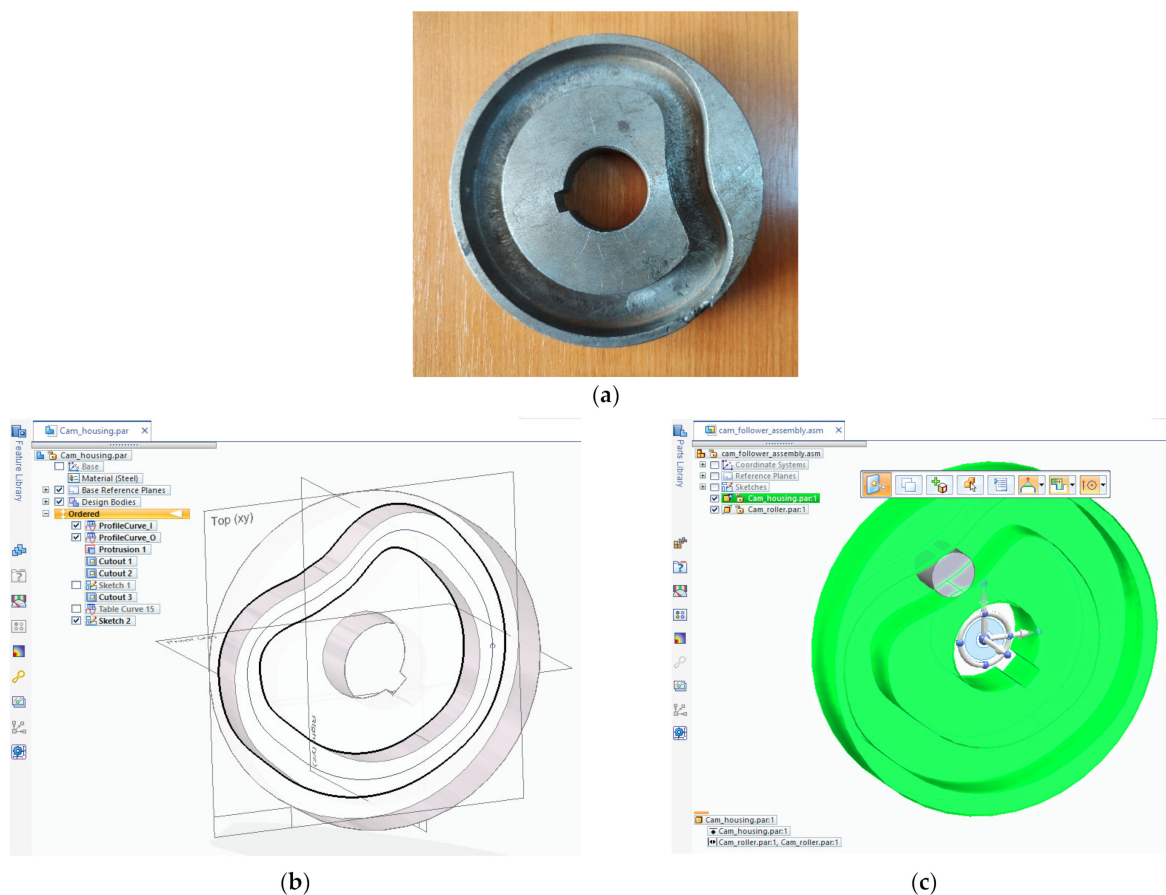


Figure 3. Images for the studied cam and CAD models: (a) photographic image of the real cam; (b) graphical representations in Siemens SolidEdge—3D view of the cam housing model; (c) graphical representations in Siemens SolidEdge—3D view of the cam-roller assembly.

The FEM (Finite Element Method) analyses were carried out under the *Ansys Transient Structural* module. The two imported part components were assigned with the 4340 type of steel, which can be found inside Ansys's material library. When in function, after many cycles, the assembly produces hardened surfaces, which can withstand higher tensile strengths and display improved fatigue resistance. Due to its similar mechanical properties, the 4340 steel was the choice to make without the need for any external files from another

material database. The motion of the follower roller had to consider a set of more than 720 data lines, including each point composing the entire path on the cam profile. In response, a new coordinate system, assigned only to the follower roller and having the same direction for each axis as the global one, was inserted in the CAE model. Connections in the model included contacts and joints. In the contacts branch, frictionless contact between the outer surface of the follower roller was set on both the lower and upper surfaces of the cam groove. The behavior of the contact between surfaces was set as asymmetric. The formulation of the contact was set to *Augmented Lagrange* with the option to update stiffness with each iteration, and there was no stabilization damping factor. The interface treatment was set to adjust for touch at all times. The *next contact pair* was assigned to the back of the follower roller and the corresponding surface of the cam groove. This component was later grounded inside the joint branch. The *next joint* was set to planar and was scoped to the outer surface of the follower roller. This gave the possibility to follow the needed path, as this type of joint allows only translations on X and Y and rotations around Z (see Figure 4a). Mesh-wise used a body sizing of 5 mm for both components and a face sizing of 1 mm for the surfaces in contact. Error limits were set to aggressive mechanical with a smooth transition between elements. When assessing the rigid body behavior, reducing the dimensions was chosen. That resulted in more than 22,000 nodes and 11,000 elements (see Figure 4b).

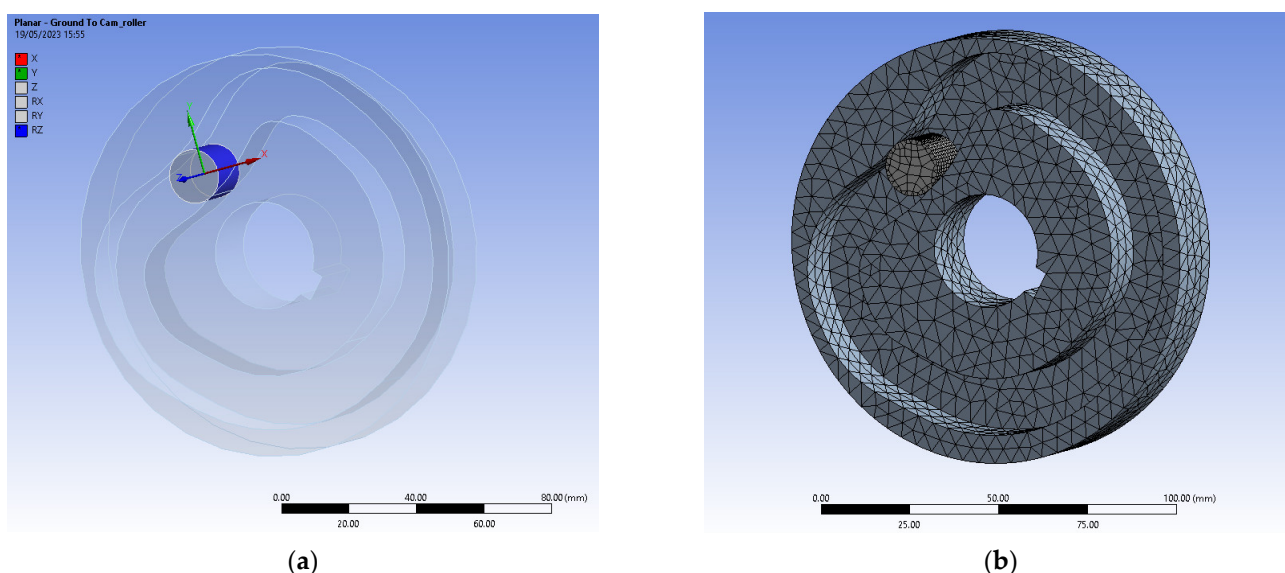


Figure 4. Setup conditions and mesh distribution: (a) planar joint scoped to the follower's outer surface; (b) 3D view of the mesh produced for the cam-roller assembly.

Analyses settings included steps for each point along the path. The large deflection option was turned on, and the un-symmetric option for Newton–Raphson computation was chosen for the nonlinear controls. No stabilization was needed. The other options were left, as the software tool implicitly controlled them. A force was used as the type of load, and three joint loads for the translation on X and Y and the rotation around Z were set.

2.4. Experimental Conditions

Validation experiments were performed to test the reliable appropriateness of the dynamic model based on elastic cam-follower contact and the simulation data. The structure of the laboratory equipment is schematically shown in Figure 5, where the symbols represent the following: 1 is the disk cam with a profiled groove, 2 is the oscillating follower, 3 is the follower roller, 4 is a slider (the yarn catcher), 5 is a slide block, 6 is the fixed element (frame), 7 is a PCB model 352A76 accelerometer, 8 is a PCB model 480CO2 amplifier, 9 is a data acquisition board, and 10 is a PC. In the same figure, VTL is a rotation speed variator

with a transmission ratio of $1/2 \div 2$, and EM is a 3-phase asynchronous electric motor with a nominal power of $P_n = 1.1$ (kW), a synchronous rotation speed of $n_{sm} = 1000$ (rpm), and a nominal rotation speed of $n_m = 920$ (rpm).

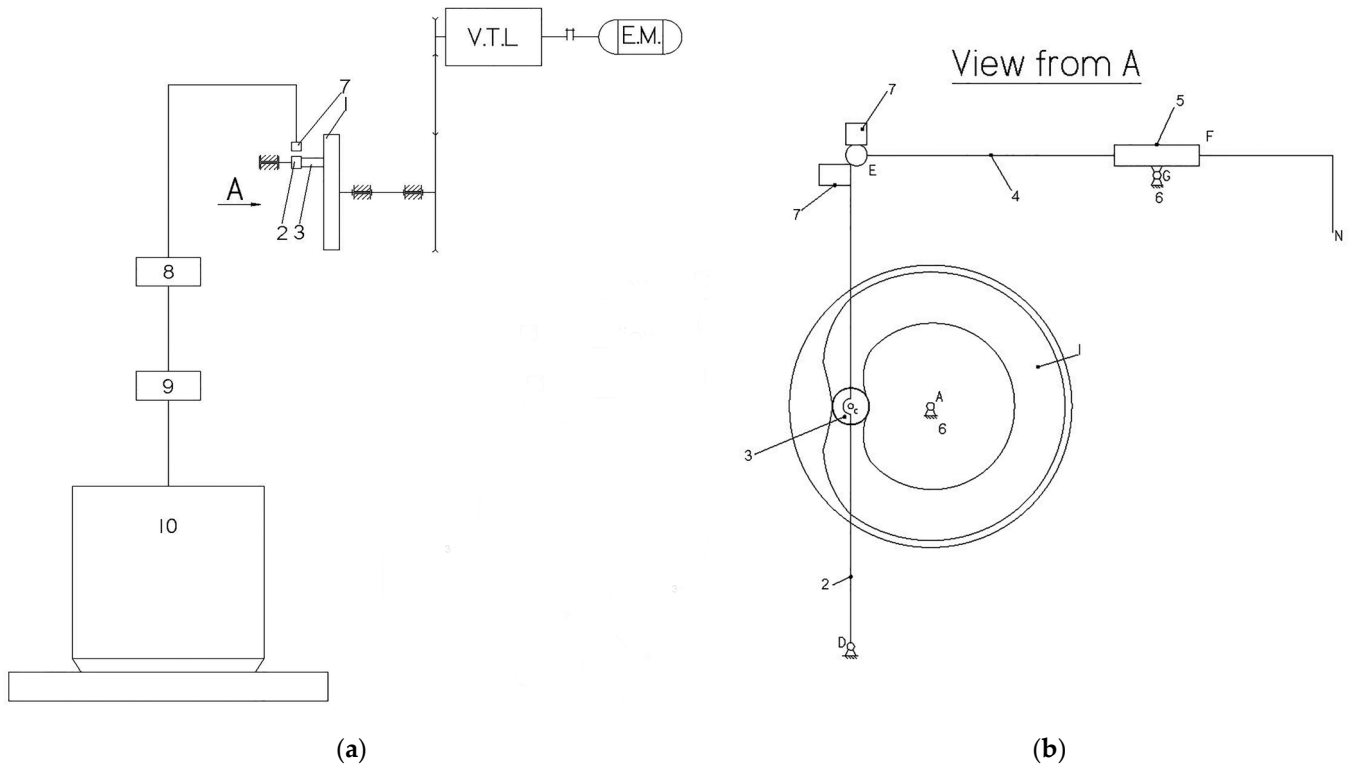


Figure 5. Structure of the experiment laboratory equipment: (a) structural diagram of the experiment stand; (b) detailed view from A with the mechanism structure detail.

The measurements were performed after the calibration on a system schematically shown in Figure 6, where the symbols are as follows: 1 is a 6V model I4103 DC power source, 2 is a B&K type 4291 electro-dynamic excitation system, which produced an acceleration of 9.81 m/s at a frequency of 79.6 Hz, 3 is the accelerometer to be calibrated, 4 is a ball device, 5 is the amplifier, 6 is an oscilloscope, 7 is the data acquisition board, and 8 is the PC. A multiplying correction factor $K_a = 86.43$ (m/s²/V) was established for translating the measured electric signals (V) into acceleration values (m/s²). The tangential and the normal accelerations for the follower, in point E, were measured.

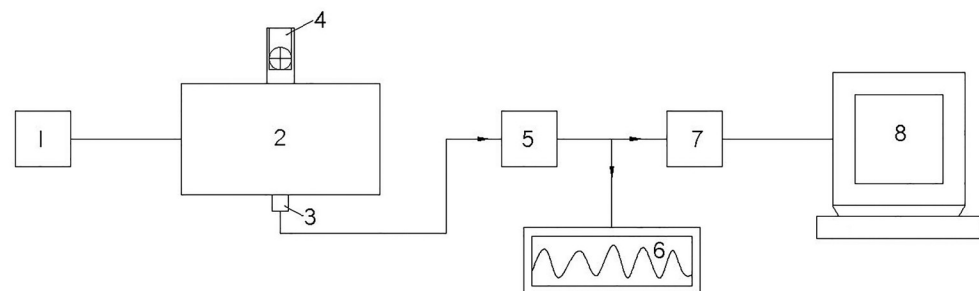


Figure 6. Structure of the calibration system.

The experimental measurements were performed for a cam with the profile having the law of motion with sine acceleration on the ascending and descending phases. The average value for the backlash in the coupling cam-follower roller was $j = 0.128$ (mm). The

active load was $F_u = 0$ (N). Measurements were taken for three values of the cam’s rotation speed, at 180, 300, and 500 rpm. The scanning frequency was set to 10,000 scans/s. The measured signal data were processed using a customized virtual instrument developed in the LabVIEW environment.

3. Results

3.1. Numerical Simulation Results

A set of numerical simulation results is exemplified in Table 2. The meanings of the symbols in the Table 2 header were explained in Section 2.2. The particular data in Table 2 correspond to the simulated experiment performed for the dynamic model with rigid elements, the cam profile with the law of motion with sine acceleration, and variable cam speed.

Table 2. Results from the numerical simulation for the dynamic model with rigid elements.

Simulation No.	$(M_{R13D})_{max}$ (Nm)	$(\varphi_{2rcj}-\varphi_{2rfj})_{max}$ (°)	$(\omega_{2rcj}-\omega_{2rfj})_{max}$ (rad/s)	$(\omega_{1rcj}-\omega_{1rfj})_{max}$ (rad/s)	$(Percussion_{int})_{max}$ (Ns)	(Jumps No.)
1: A1B1C1D1	5	0.04	0.66	0.016	0.17	15
2: A1B1C1D2	20.4	0.035	0.673	0.0657	0.69	15
3: A1B1C2D1	13.75	0.05	1.16	0.08	0.28	15
4: A1B1C2D2	54.22	0.0347	1.1104	0.3046	1.1102	15
5: A1B2C1D1	5	0.1	1.25	0.025	0.305	6
6: A1B2C1D2	20.45	0.1215	1.216	0.1051	1.225	6
7: A1B2C2D1	13.75	0.1	2	0.13	0.51	6
8: A1B2C2D2	54.22	0.121	1.9	0.524	1.94	7
9: A2B1C1D1	17	0	0	0	0	0
10: A2B1C1D2	32.39	0.01514	0.389	0.01587	0.383	33
11: A2B1C2D1	26.25	0.00141	0.164	0.00225	0.042	38
12: A2B1C2D2	65.85	0.0151	0.762	0.178	0.753	22
13: A2B2C1D1	17	0	0	0	0	0
14: A2B2C1D2	32.39	0.12	1.088	0.0438	1.045	16
15: A2B2C2D1	26.25	0.0106	0.298	0.01	0.075	13
16: A2B2C2D2	65.85	0.1196	2.024	0.42	2.008	5

As graphical representations for the numerical simulation results, some examples are given below in relation to the above-mentioned experimental conditions valid in Table 2. Figure 7 shows the time dependencies for the parameter (M_{R13D}) for two simulated situations: simulation No. 10 in Table 2, where the jump occurs (sign change) (Figure 7a), and simulation No. 13 in Table 2, where no jump occurs (no sign change) (Figure 7b).

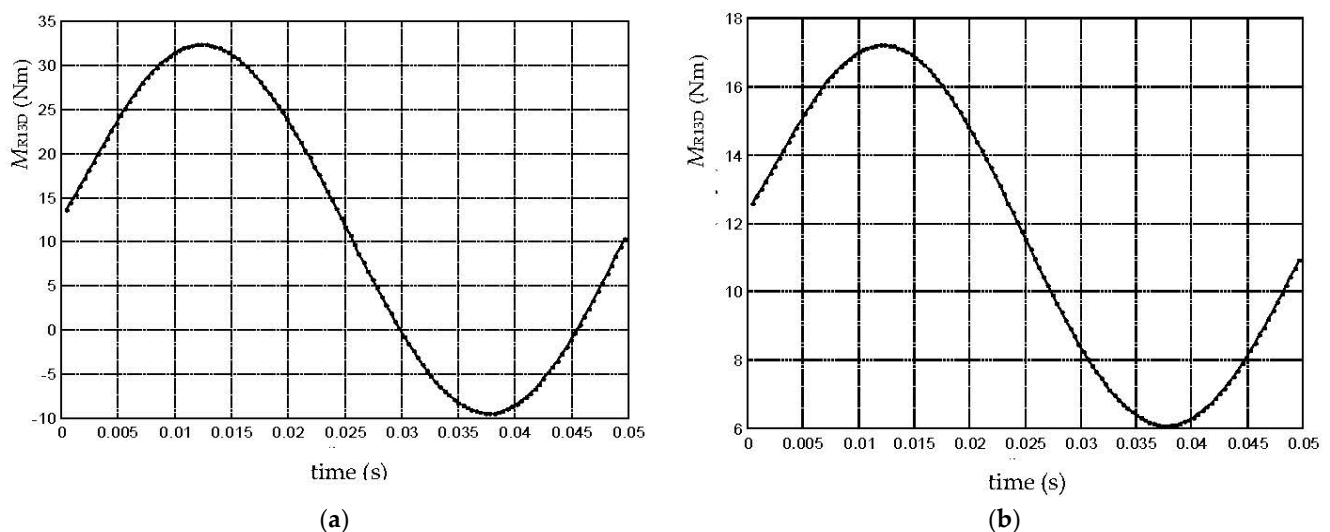


Figure 7. Time dependencies for parameter M_{R13D} : (a) jump situation; (b) no jump situation.

Figure 8 shows the time dependencies for the other indicators of the jump phenomenon parameters $(\varphi_{2rcj}-\varphi_{2rfj})$, $(\omega_{2rcj}-\omega_{2rfj})$, $(\omega_{1rcj}-\omega_{1rfj})$, and $(Percussion_{int})$ for the same situation as simulation No. 10 in Table 2 and the following values of the input parameters (see also Table 1): $F_u = 65$ (N), $j = 0.016$ (mm), $n_1 = 180$ (rpm), and $J_t = 4 \cdot J_t$.

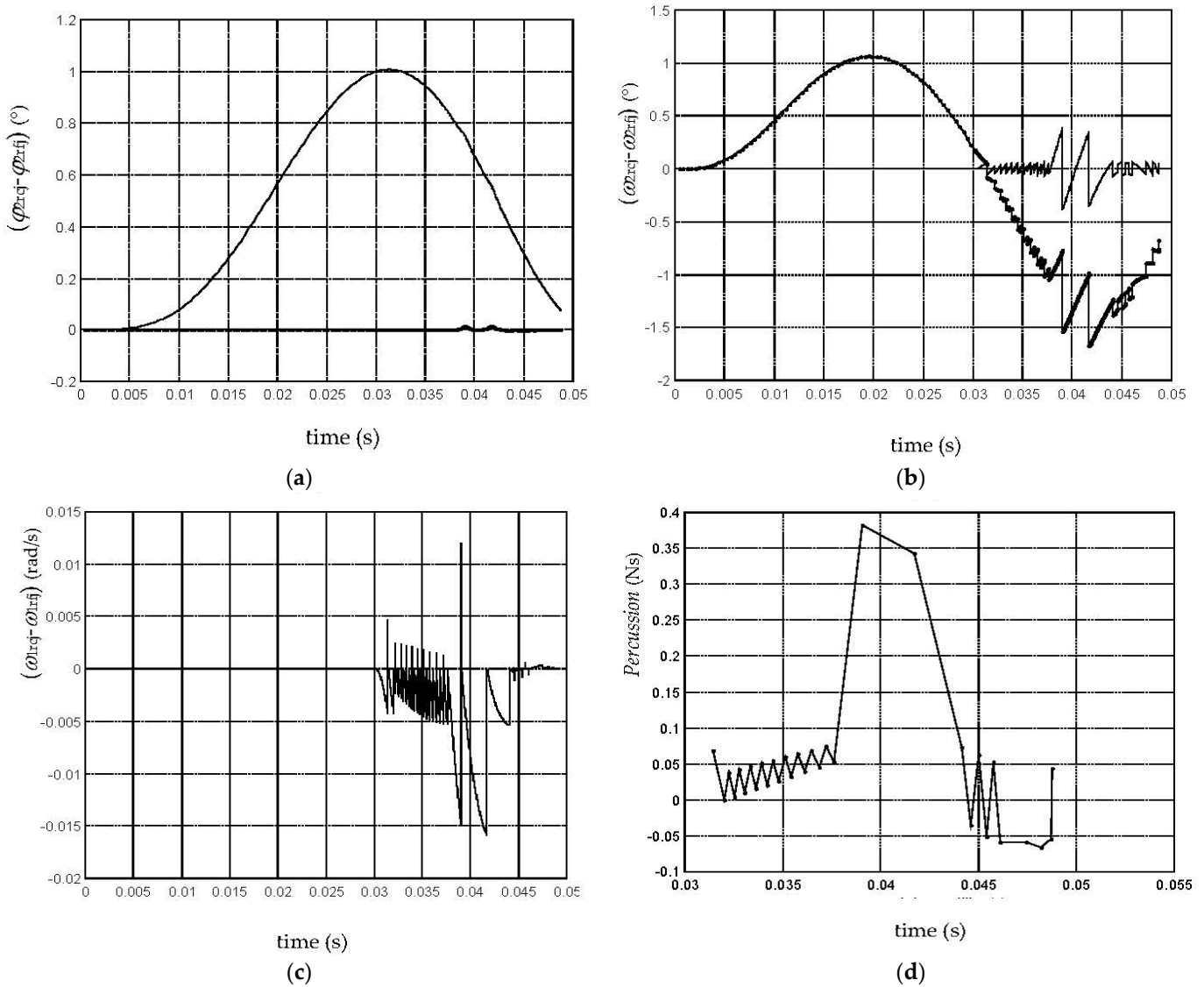


Figure 8. Time dependencies for jump phenomenon indicators: (a) dependency of $(\varphi_{2rcj}-\varphi_{2rfj})$; (b) dependency of $(\omega_{2rcj}-\omega_{2rfj})$; (c) dependency of $(\omega_{1rcj}-\omega_{1rfj})$; (d) dependency of $(Percussion_{int})$.

Results data from the 2^4 simulated experiments have been mathematically modeled in matrix form following the ANOVA method using customized developed calculation MS Excel sheets. The chosen variance analysis computation was based on Fisher's criterion.

The reduced matrix empirical models containing only the significant effects for the investigated parameters $(M_{R13D})_{max}$, $(\varphi_{2rcj}-\varphi_{2rfj})_{max}$, $(\omega_{2rcj}-\omega_{2rfj})_{max}$, $(\omega_{1rcj}-\omega_{1rfj})_{max}$, $(Percussion_{int})_{max}$, and $(Jumps\ no.)$ are exemplified as follows:

$$\begin{aligned} (M_{R13D})_{max} = & 29.3606 + \begin{bmatrix} -6.0118 & 6.0118 \end{bmatrix} \times [A_A] + \begin{bmatrix} -10.656875 & 10.656875 \end{bmatrix} \times [A_C] \\ & + \begin{bmatrix} -13.860625 & 13.860625 \end{bmatrix} \times [A_D] + {}^t[A_C] \times \begin{bmatrix} 6.156875 & -6.156875 \\ -6.156875 & 6.156875 \end{bmatrix} \times [A_D] \end{aligned} \quad (20)$$

$$(\varphi_{2rcj} - \varphi_{2rfj})_{\max} = 0.05525 + [0.020022 \ -0.020022] \times [A_A] + [\ -0.03133 \ 0.03133] \times [A_B] + [\ -0.0175 \ 0.0175] \times [A_D] + {}^t[A_A] \times \begin{bmatrix} 0.0147 & -0.0147 \\ -0.0147 & 0.0147 \end{bmatrix} \times [A_D] + {}^t[A_B] \times \begin{bmatrix} 0.0164 & -0.0164 \\ -0.0164 & 0.0164 \end{bmatrix} \times [A_D] \tag{21}$$

$$(\omega_{2rcj} - \omega_{2rfj})_{\max} = 0.9184 + [0.327775 \ -0.327775] \times [A_A] + [-0.3036 \ 0.3036] \times [A_B] + [\ -0.2589 \ 0.2589] \times [A_C] + [\ -0.2269 \ 0.2269] \times [A_D] + {}^t[A_A] \times \begin{bmatrix} 0.248225 & -0.248225 \\ -0.248225 & 0.248225 \end{bmatrix} \times [A_D] \tag{22}$$

$$(\omega_{1rcj} - \omega_{1rfj})_{\max} = 0.12002 + [0.03628 \ -0.03628] \times [A_A] + [-0.03721 \ 0.03721] \times [A_B] + [-0.08608 \ 0.08608] \times [A_C] + [\ -0.08711 \ 0.08711] \times [A_D] + {}^t[A_B] \times \begin{bmatrix} 0.027676 & -0.027676 \\ -0.027676 & 0.027676 \end{bmatrix} \times [A_D] + {}^t[A_C] \times \begin{bmatrix} 0.06343 & -0.06343 \\ -0.06343 & 0.06343 \end{bmatrix} \times [A_D] + {}^t[A_D] \times \begin{bmatrix} 0.028873 & -0.028873 \\ -0.028873 & 0.028873 \end{bmatrix} \times [A_D] \tag{23}$$

$$(\text{Percussion}_{\text{int}})_{\max} = 0.6585 + [0.1202 \ -0.1202] \times [A_A] + [-0.2299 \ 0.2299] \times [A_B] + [-0.1812 \ 0.1812] \times [A_C] + [\ -0.4857 \ 0.4857] \times [A_D] + {}^t[A_B] \times \begin{bmatrix} 0.1802 & -0.1802 \\ -0.1802 & 0.1802 \end{bmatrix} \times [A_D] + {}^t[A_C] \times \begin{bmatrix} 0.1272 & -0.1272 \\ -0.1272 & 0.1272 \end{bmatrix} \times [A_D] \tag{24}$$

$$(\text{Jumps no.}) = 13.25 + [\ -2.625 \ 2.625] \times [A_A] + [\ 5.875 \ -5.875] \times [A_B] + [\ -1.875 \ 1.875] \times [A_C] \tag{25}$$

Another set of numerical simulation results corresponding to the simulated experiment performed for the dynamic model with elastic contact, for the cam profile with the law of motion with sine acceleration and variable cam speed is further exemplified in Table 3. The symbols in Table 3 represent the parameters presented in Section 2.2.

Table 3. Results from the numerical simulation for the dynamic model with elastic contact.

Simulation No.	(M_{R13D})max (Nm)	(M_{R13D})min (Nm)	(x_{el})max (mm)	(x_{el})min (mm)	(Jumps no.)	(Impacts no.)
1: A1B1C1D1	5.161	-5.193	0.0075	-0.0006	1	0
2: A1B1C1D2	20.451	-20.976	0.0107	-0.0025	1	0
3: A1B1C2D1	13.98	-14.327	0.0109	-0.0018	1	0
4: A1B1C2D2	54.233	-58.552	0.0071	-0.0051	1	0
5: A1B2C1D1	5.161	-5.193	0.0075	-0.0006	1	0
6: A1B2C1D2	20.451	-20.976	0.0107	-0.0025	1	0
7: A1B2C2D1	13.98	-14.327	0.0109	-0.0018	1	0
8: A1B2C2D2	54.233	-58.552	0.0071	-0.0051	1	0
9: A2B1C1D1	17.211	6.078	-0.0004	-0.0015	0	0
10: A2B1C1D2	32.388	-9.476	0.0075	-0.0034	1	0
11: A2B1C2D1	25.932	-2.805	0.0053	-0.0027	1	0
12: A2B1C2D2	65.85	-46.058	0.0065	-0.006	1	0
13: A2B2C1D1	17.211	6.078	-0.0004	-0.0015	0	0
14: A2B2C1D2	32.388	-9.476	0.0075	-0.0034	1	0
15: A2B2C2D1	25.932	-2.805	0.0053	-0.0027	1	0
16: A2B2C2D2	65.85	-46.058	0.0065	-0.006	1	0

Graphical representations for the numerical simulation results are given in Table 3 and examples are given in Figure 9, where the time dependencies for the parameters (M_{R13D}) and (x_{el}) are shown corresponding to simulation No. 1 in Table 3, where the jump occurs (sign change) in the following input conditions: $F_u = 0$ (N), $j = 0.016$ (mm), $n_1 = 180$ (rpm), and $J_t = 1 \cdot J_t$.

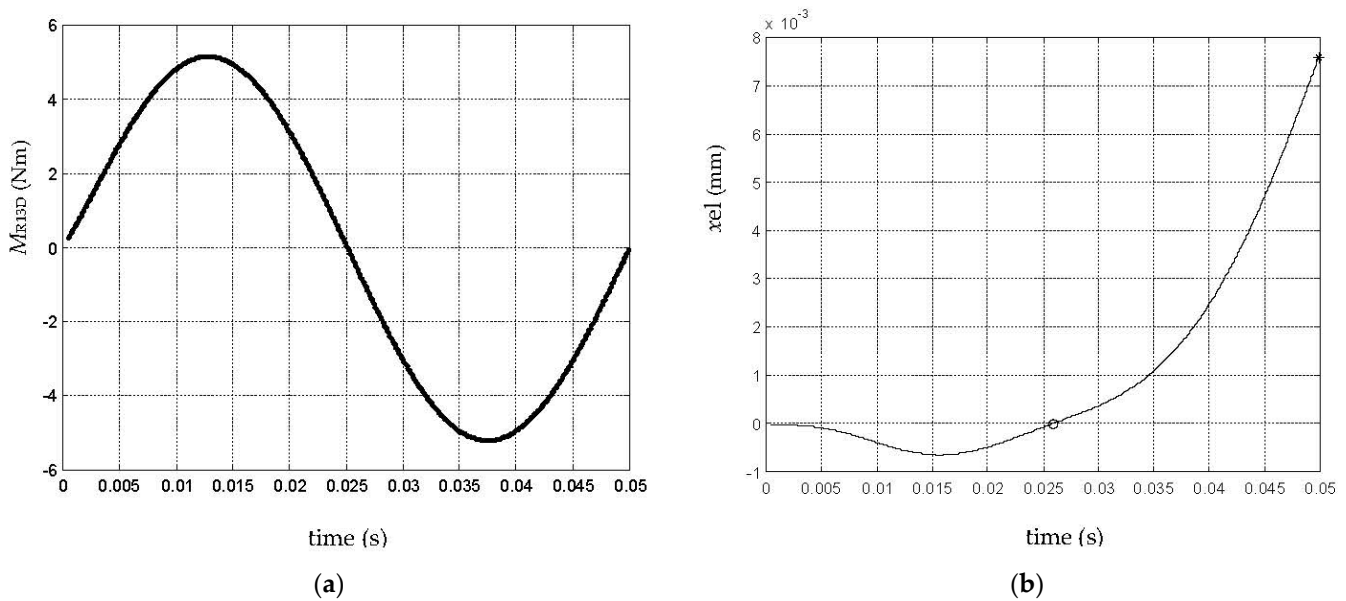


Figure 9. Time dependencies for jump phenomenon indicators: (a) dependency of (M_{R13D}) ; (b) dependency of (x_{el}) .

The reduced matrix empirical models containing only the significant effects for the investigated parameters $(M_{R13D})_{\max}$, $(x_{el})_{\max}$, and $(Jumps\ no.)$ are exemplified in Equations (26)–(28).

$$(M_{R13D})_{\max} = 29.4007 + \begin{bmatrix} -5.9445 & 5.9445 \end{bmatrix} \times [A_A] + \begin{bmatrix} -10.598 & 10.598 \end{bmatrix} \times [A_C] + \begin{bmatrix} -13.829 & 13.829 \end{bmatrix} \times [A_D] + {}^t[A_A] \times \begin{bmatrix} -0.0522 & 0.0522 \\ 0.0522 & -0.0522 \end{bmatrix} \times [A_C] + {}^t[A_A] \times \begin{bmatrix} -0.056 & 0.056 \\ 0.056 & -0.056 \end{bmatrix} \times [A_D] + {}^t[A_C] \times \begin{bmatrix} 6.213 & -6.213 \\ -6.213 & 6.213 \end{bmatrix} \times [A_D] \quad (26)$$

$$(x_{el})_{\max} = 0.00688 + \begin{bmatrix} 0.00216 & -0.00216 \end{bmatrix} \times [A_A] + \begin{bmatrix} -0.00056 & 0.00056 \end{bmatrix} \times [A_C] + \begin{bmatrix} -0.00106 & 0.00106 \end{bmatrix} \times [A_D] + {}^t[A_A] \times \begin{bmatrix} 0.00061 & -0.00061 \\ -0.00061 & 0.00061 \end{bmatrix} \times [A_C] + {}^t[A_A] \times \begin{bmatrix} 0.00121 & -0.00121 \\ -0.00121 & 0.00121 \end{bmatrix} \times [A_D] + {}^t[A_C] \times \begin{bmatrix} -0.00171 & 0.00171 \\ 0.00171 & -0.00171 \end{bmatrix} \times [A_D] \quad (27)$$

$$(Jumps\ no.) = 0.875 + \begin{bmatrix} 0.125 & -0.125 \end{bmatrix} \cdot [A_A] + \begin{bmatrix} -0.125 & 0.125 \end{bmatrix} \cdot [A_C] + \begin{bmatrix} -0.125 & 0.125 \end{bmatrix} \cdot [A_D] + {}^t[A_A] \cdot \begin{bmatrix} 0.125 & -0.125 \\ -0.125 & 0.125 \end{bmatrix} \cdot [A_C] + {}^t[A_A] \cdot \begin{bmatrix} 0.125 & -0.125 \\ -0.125 & 0.125 \end{bmatrix} \cdot [A_D] + {}^t[A_C] \cdot \begin{bmatrix} -0.125 & 0.125 \\ 0.125 & -0.125 \end{bmatrix} \cdot [A_D] \quad (28)$$

3.2. FEA Results

FEA results included a contact tool that revealed the contact status between the investigated surfaces in coupling and gap distribution. The status tool shows that the sticking line is pretty thin compared to the sliding area (see Figure 10a), which indicated a possible gap. That was confirmed when accessing gap results (see Figure 10b). One could observe that the follower roller is not touching the cam housing along its entire length but as it moved, small gaps were recorded. Gap peaks of about -0.0045 mm were highlighted on the sticking line, and such results were consistent with the ones obtained in the numerical simulation. The surrounding surfaces not in direct contact registered greater values. This type of result helped in proving the FEA research setups. Figure 10c shows the deformation in all three directions (e.g., total deformation) for the follower roller.

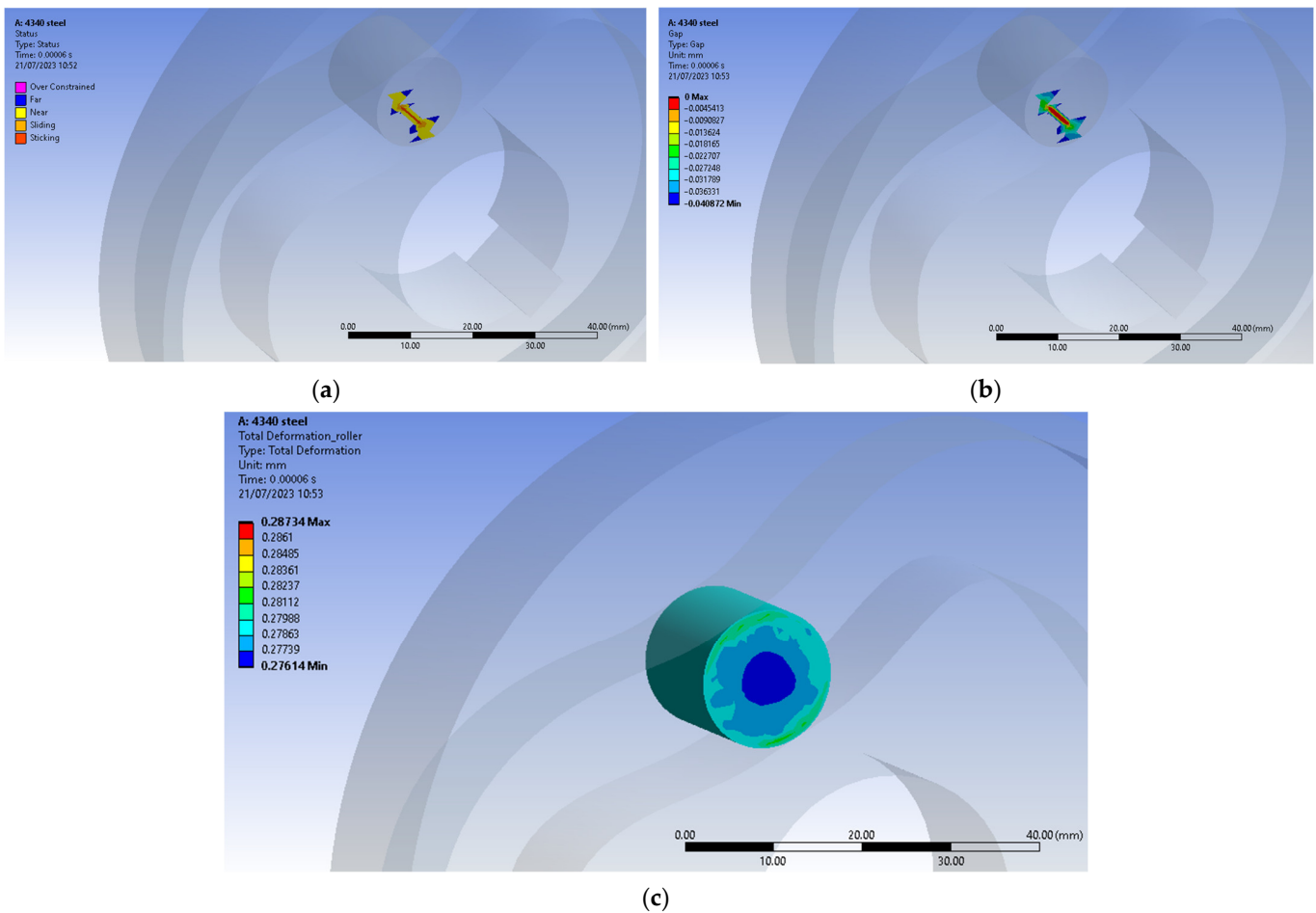
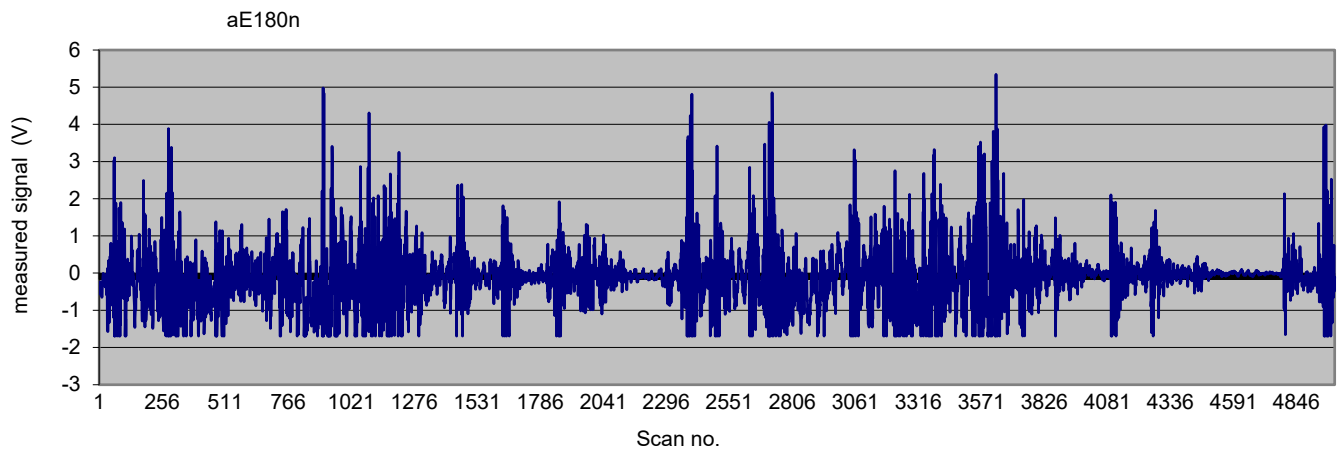


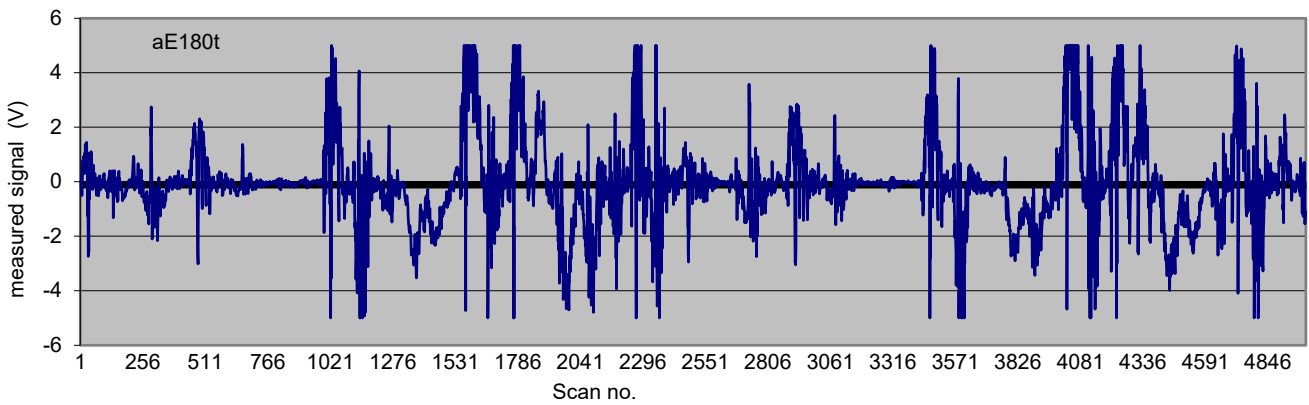
Figure 10. FEA results: (a) graphical representation of the contact status distribution; (b) graphical representation of the gap distribution; (c) total deformation plots of the roller—detail.

3.3. Experimental Results

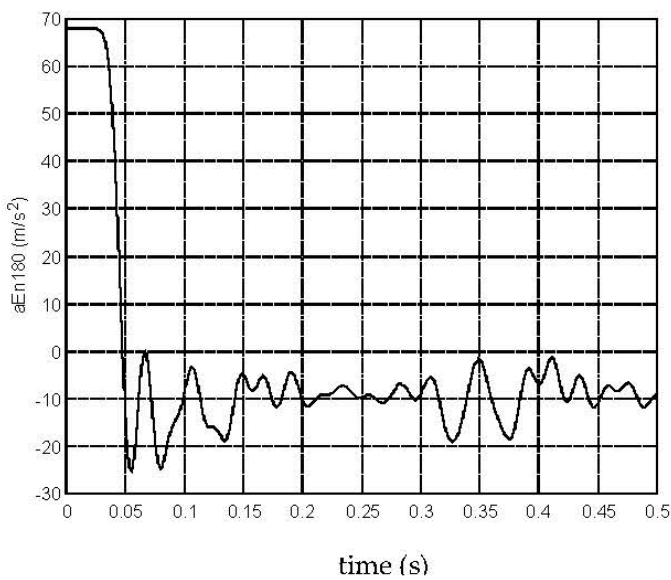
Some of the registered measured data are exemplified in Figure 11. The spectrum of the measured signal values together with the time spectrum of the filtered and translated data for the normal acceleration of follower a_{E180n} and the tangential acceleration of follower a_{E180t} are shown, corresponding to a rotation speed of 180 rpm for the cam. Experimental results were compared with those obtained by the numerical simulation in the manner exemplified in the charts in Figures 12–14, corresponding to a rotation speed of 180 rpm for the cam in the experiment. The cam's rotation speed ω_1 constant and variable in the numerical simulation were considered in the comparative representations. In Figures 12 and 13, the angular velocity ω_2 of the follower (rad/s) for three cases is on the y -axis: numerical simulation with the dynamic model for the angular velocity of the cam ω_1 constant (denoted in chart $w1 = ct.$), numerical simulation with the dynamic model for the angular velocity of the cam ω_1 variable (denoted in chart $w1 = var.$), and the experimentally measured values of velocity ω_2 of the follower (measured values). In Figure 14, the angular acceleration ε_2 of the follower (in rad/s^2) for three cases is on the y -axis: numerical simulation with the dynamic model for the angular velocity of the cam ω_1 constant (denoted in chart $w1 = ct.$), numerical simulation with the dynamic model for the angular velocity of the cam ω_1 variable (denoted in chart $w1 = var.$), and the experimentally measured values of acceleration ε_2 of the follower (measured values).



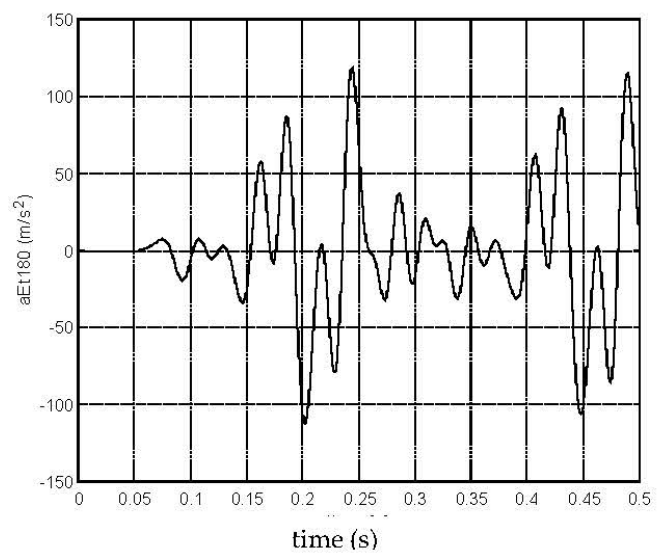
(a)



(b)



(c)



(d)

Figure 11. Experimental results: (a) spectrum of the measured signal values for a_{E180n} ; (b) spectrum of the measured signal values for a_{E180t} ; (c) time spectrum of the filtered and translated data for a_{E180n} ; (d) time spectrum of the filtered and translated data for a_{E180t} .

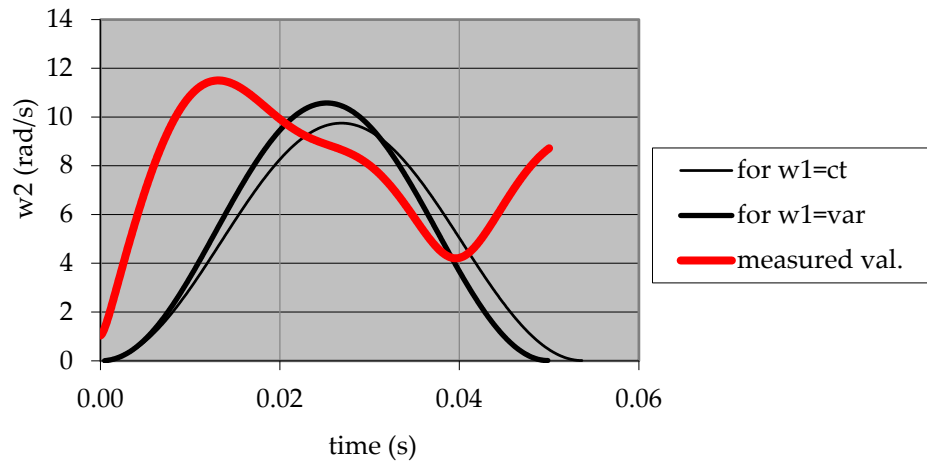


Figure 12. Comparative representation for the time evolution of the angular velocity ω_2 of the follower for the numerical simulation on the dynamic model with the elastic contact vs. experiment.

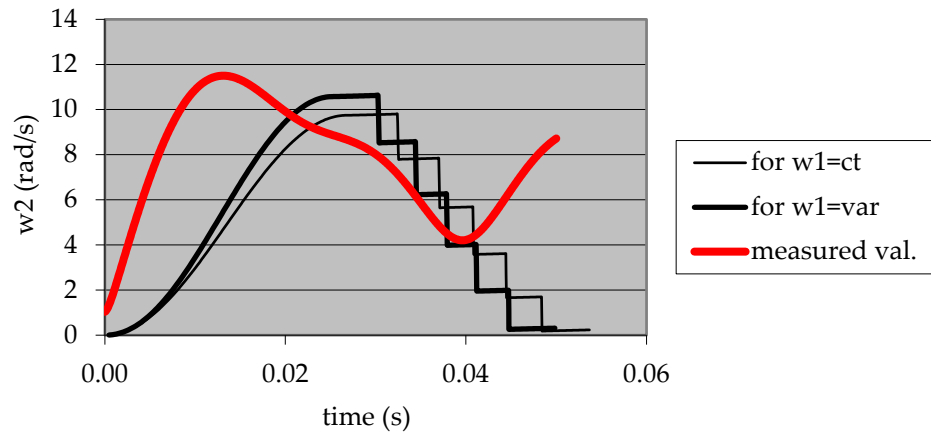


Figure 13. Comparative representation for the time evolution of the angular velocity ω_2 of the follower for the numerical simulation on the dynamic model with rigid elements vs. experiment.

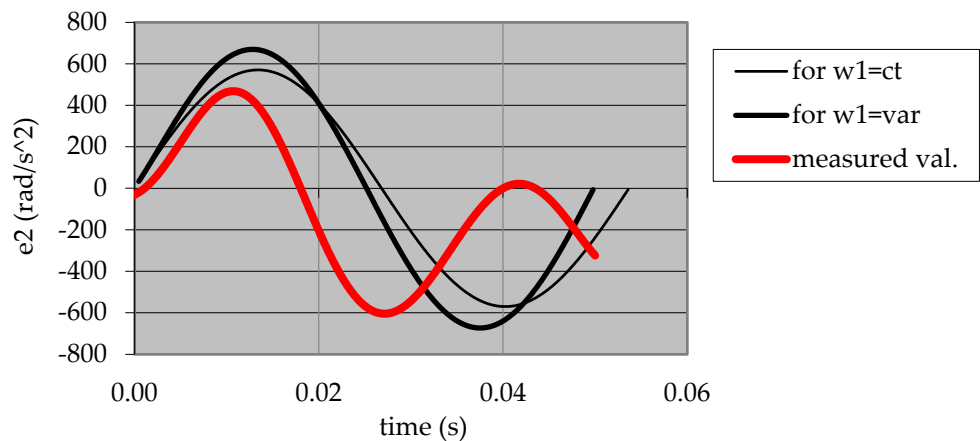


Figure 14. Comparative representation for the time evolution of the angular acceleration ϵ_2 of the follower for the numerical simulation on the dynamic model with the elastic contact vs. experiment.

4. Discussion

Simulation tests on the proposed theoretical dynamic models returned a great amount of data and information regarding the influences of the geometrical parameters and the

technological conditions on the investigated indicators of the jump phenomenon in contact loss for the studied cam-follower mechanism.

The numerical simulation results for the dynamic model with rigid elements highlighted more than one follower jump and impact during the rising phase of the follower. The acceleration jumps for the follower at its impact with the cam is theoretically infinite because modeling the impact was considered instantaneous.

Regarding the influences of the input parameters F_u , j , n_1 , and J_t on the investigated jump phenomenon indicators, the simulation results for the dynamic model with rigid elements showed the following: bigger values for F_u , n_1 , and J_t determined bigger values for $(M_{R13D})_{\max}$, bigger values for j and J_t determined bigger values for $(\varphi_{2rcj}-\varphi_{2rfj})_{\max}$, bigger values for F_u determined smaller values for $(\varphi_{2rcj}-\varphi_{2rfj})_{\max}$, bigger values for j , n_1 , and J_t determined bigger values for $(\omega_{2rcj}-\omega_{2rfj})_{\max}$, bigger values for F_u determined smaller values for $(\omega_{2rcj}-\omega_{2rfj})_{\max}$, bigger values for n_1 and J_t determined bigger values for $(\omega_{1rcj}-\omega_{1rfj})_{\max}$, bigger values for F_u determined smaller values for $(\omega_{1rcj}-\omega_{1rfj})_{\max}$, bigger values for j , n_1 , and J_t determined bigger values for $(Percussion_{int})_{\max}$, bigger values for F_u determined smaller values for $(Percussion_{int})_{\max}$, bigger values for F_u and n_1 determined bigger values for $(Jumps\ no.)$, and bigger values for j determined smaller values for $(Jumps\ no.)$.

One could conclude that the increase in F_u values diminishes the negative dynamic effects related to contact loss, as effects of j , n_1 , and J_t are the opposite. In order to avoid the jump of the follower, it appeared necessary to increase F_u and decrease the speed of the cam and the generalized mass of the follower.

For the law of motion with sine acceleration, the jump occurred at a lower cam speed than for the law of motion with cosine acceleration. That was because the law of motion with sine acceleration had absolute values of acceleration bigger than the law of motion with cosine acceleration [52].

The numerical simulations for the dynamic model with elastic contact highlighted the following: bigger values for F_u , n_1 , and J_t resulted in bigger values for $(M_{R13D})_{\max}$, bigger values for n_1 and J_t resulted in bigger values for $(x_{el})_{\max}$, bigger values for F_u resulted in smaller values for $(x_{el})_{\max}$, bigger values for n_1 and J_t resulted in bigger values for $(Jumps\ no.)$, and bigger values for F_u resulted in smaller values for $(Jumps\ no.)$. The input parameter j did not prove a significant effect on any of the investigated jump phenomenon indicators, $(M_{R13D})_{\max}$, $(x_{el})_{\max}$, or $(Jumps\ no.)$, which could be explained by the fact that no impact resulted in the rising phase of the follower.

One could conclude again that for the dynamic model with elastic contact, the increase in F_u values diminished the negative dynamic effects related to contact loss, and the effects of n_1 and J_t were the opposite. For the law of motion with sine acceleration, the jump occurred at a lower cam speed than for the law of motion with cosine acceleration, which is again a valid conclusion.

By comparing the simulation results for the two dynamic models, one could observe significant differences regarding the indicator $(Jumps\ no.)$. The explanation could be found in the fact that at the beginning of the rising phase, a so-named *deepening* of the follower into the cam's profile, eventually followed by the contact loss and jump, occurred. The important effect of the cam-follower contact elasticity is, therefore, highlighted.

Related to the FEA results, one could conclude that the graphical distribution of gap occurrences may help in optimizing the CAE model considering various scenarios.

Experimental data highlighted that the dynamic model with elastic contact delivered results closer to the experiment, mainly regarding the number of jumps and impacts.

A comparison of the experimental results for different values of the cam speed led to the conclusion that the negative dynamic effects are bigger for bigger values of the cam speed.

The registered differences between the simulation data and the experimental data resulted from the nature of the simplifying hypotheses assumed in modeling.

5. Conclusions

Within the broad context of cam mechanism dynamics research, the influence of the backlash from the higher kinematic pair cam-follower was less studied, mainly for the situation of the mechanisms with a disk cam with a profiled groove and an oscillating follower. Such a mechanism from an automated feeding system of a textile machine was studied within the presented research approach. Although the customized research details and results were specific to the particular studied mechanism, the approach has general validity and can be extended to other situations in this class of mechanisms.

Theoretical dynamic modeling and simulation of the complex phenomena in cam mechanism dynamics may deliver important reliable information that is useful for predicting the quality and efficiency in real process operation. The idea to develop two dynamic models, one considering rigid elements in contact and the second considering elastic cam-follower contact, highlights the influence of the cam-follower contact elasticity on the jump phenomenon.

Hypotheses of theoretical dynamic modeling excluding the influence of factors, such as friction in kinematic couplings, the masses and the inertia moments of the kinematic elements of the driving chain from the electrical motor up to the camshaft, the rotational kinetic energy for the follower roller, and the elasticity of the other elements of the mechanism, resulted in limitations of the theoretical models in accurately predicting the specific dynamic behavior.

The models were tested within a simulated experiment, and numerical simulation results evidenced the influence of input factors like the applied load on the mechanism, the backlash in the higher kinematic pair cam-follower, the rotational speed of the cam, the inertia moment reduced to the follower, and some indicators of the jump phenomenon.

The importance of theoretical modeling and simulation is given by the unlimited number of input conditions that can be simulated, as presented above in Sections 2.2 and 3.1, for obtaining valuable referential data in experiment planning or real operation behavior predicting.

The FEA research approach delivered important results that were helpful in the virtual testing of the dynamic models. However, it is recommended that the FEA-obtained results may be used with care since it was acknowledged that further refinement is necessary in terms of mesh quality and setup conditions.

Validation experiments were performed, proving the reliable appropriateness of the dynamic model based on the elastic cam-follower contact. Experimental values for the investigated dynamic parameters confirmed the research hypotheses and expectations.

In the future, a more in-depth theoretical approach for developing a more relevant dynamic modeling algorithm and extended FEA approaches will concern the authors. These will be intended to reduce the simplifying hypotheses and consider other influence factors such as friction, thermal phenomena, material elasticity, etc.

Author Contributions: Conceptualization, E.M. and V.M.; methodology, E.M. and A.M.M.; software, E.M., V.M. and A.M.M.; validation, E.M. and G.N.; formal analysis, G.N.; investigation, E.M., V.M. and A.M.M.; resources, L.L.T.; data curation, E.M., V.M. and A.M.M.; writing—original draft preparation, E.M. and V.M.; writing—review and editing, V.M.; visualization, M.I.R. and L.L.T.; supervision, E.M.; project administration, V.M. All authors have read and agreed to the published version of the manuscript.

Funding: This research received no external funding.

Data Availability Statement: Data are available upon request from the authors.

Conflicts of Interest: The authors declare no conflict of interest.

References

1. Ungureanu, L.M.; Petrescu, F.I.T. Dynamics of Mechanisms with Superior Couplings. *Appl. Sci.* **2021**, *11*, 8207. [[CrossRef](#)]
2. Minárik, M.; Bodnár, F. Dynamic Analysis of the Crank Mechanism through the Numerical Solution. *Manuf. Technol.* **2019**, *19*, 1003–1009. [[CrossRef](#)]

3. Chen, Y.; Yu Sun, Y.; Chen, C. Dynamic analysis of a planar slider-crank mechanism with clearance for a high speed and heavy load press system. *Mech. Mach. Theory* **2016**, *9*, 81–100. [[CrossRef](#)]
4. Petrescu, R.V.; Aversa, R.; Akash, B.; Bucinell, R.; Corchado, J.; Kozaitis, S.P.; Abu-Lebdeh, T.M.; Antonio Apicella, A.; Petrescu, F.I.T. Dynamics of Mechanisms with Cams Illustrated in the Classical Distribution. *Am. J. Eng. Appl. Sci.* **2017**, *10*, 551–567. [[CrossRef](#)]
5. Wang, J.; Tan, X. A dynamic model for tail-actuated robotic fish with drag coefficient adaptation. *Mechatronics* **2013**, *23*, 659–668. [[CrossRef](#)]
6. Merticaru, E.; Merticaru, V.V. A dynamic study of a complex gear transmission. *IOP Conf. Ser. Mater. Sci. Eng.* **2020**, *997*, 012078. [[CrossRef](#)]
7. Incerti, G. Mechanical Vibrations of cam Mechanisms Driven by Asynchronous Motors: A Mathematical Model for Dynamic Analysis. In Proceedings of the ISMA2004, Leuven, Belgium, 20–22 September 2004.
8. Merticaru, E.; Merticaru, V.V. *Elements of Cam Mechanisms' Dynamics*; VIE: Iași, Romania, 1999; pp. 9–27. ISBN 973-99048-0-7. (In Romanian)
9. Norton, R.L. Modeling Cam-Follower Systems. In *Cam Design and Manufacturing Handbook*, 2nd ed.; Industrial Press, Inc.: New York, NY, USA, 2009; pp. 263–314.
10. Merticaru, E.; Merticaru, V.V. *Dynamic Phenomena in Cams Mechanisms*; Performantica: Iași, Romania, 2004; pp. 4–9. ISBN 973-730-019-X. (In Romanian)
11. Tiboni, M.; Amici, C.; Bussola, R. Cam Mechanisms Reverse Engineering Based on Evolutionary Algorithms. *Electronics* **2021**, *10*, 3073. [[CrossRef](#)]
12. Faxin, L.; Xianzhang, F. The Design of Parallel Combination for Cam Mechanism. *Proc. Environm. Sci.* **2011**, *10*, 1343–1349. [[CrossRef](#)]
13. Mohan Kumar, S.; Dhande, S.G.; Muju, M.K. Computer-Aided Design of Work Dependent Cams for Single Spindle Automats. *Mech. Mach. Theory* **1989**, *24*, 463–471. [[CrossRef](#)]
14. Petrescu, F.I.; Petrescu, R.V. Cam Dynamic Synthesis. *Al-Khwarizmi Eng. J.* **2014**, *10*, 1–23.
15. Kim, J.H.; Ahn, K.Y.; Kim, S.H. Optimal synthesis of a spring-actuated cam mechanism using a cubic spline. *Proc. Inst. Mech. Eng. Part C J. Mech. Eng. Sci.* **2002**, *216*, 875–883. [[CrossRef](#)]
16. Merticaru, E. Contributions Regarding the Dynamic Behavior of Cam Mechanisms. Ph.D. Thesis, Gheorghe Asachi Technical University, Iași, Romania, 2003. (In Romanian)
17. Naskar, T.K.; Acharyya, S. Measuring cam—Follower performance. *Mech. Mach. Theory* **2010**, *45*, 678–691. [[CrossRef](#)]
18. Yoon, K.; Rao, S.S. Cam Motion Synthesis Using Cubic Splines. *J. Mech. Des.* **1993**, *115*, 441–446. [[CrossRef](#)]
19. Müller, M.; Hüsing, M.; Beckermann, A.; Corves, B. Linkage and Cam Design with Mechanism Developer (MechDev). In Proceedings of the 25th Jc-IFTOMM Symposium, Kanagawa, Japan, 25–26 October 2019.
20. Nguyen, T.T.N. Motion Design of Cam Mechanisms by Using Non-Uniform Rational B-Spline. Ph.D. Thesis, RWTH Aachen University, Aachen, Germany, July 2018.
21. Sadek, K.S.H.; Daadbin, A. Modelling of a Torsion Bar Cam Mechanism. *Mech. Mach. Theory* **1993**, *28*, 631–640. [[CrossRef](#)]
22. Bagci, C.; Kurnool, S. Exact Response Analysis and Dynamic Design of Cam-Follower Systems Using Laplace Transforms. *J. Mech. Des.* **1997**, *119*, 359–369. [[CrossRef](#)]
23. De Groote, W.; Van Hoecke, S.; Crevecoeur, G. Prediction of follower jumps in cam-follower mechanisms: The benefit of using physics-inspired features in recurrent neural networks. *Mech. Syst. Signal Proc.* **2022**, *166*, 108453. [[CrossRef](#)]
24. Sadler, J.P.; Yang, Z. Optimal Design of Cam-Linkage Mechanism for Dynamic Force Characteristics. *Mech. Mach. Theory* **1990**, *25*, 41–57. [[CrossRef](#)]
25. Hejma, P.; Svoboda, M.; Kampo, J.; Soukup, J. Analytic analysis of a cam mechanism. *Procedia Eng.* **2017**, *177*, 3–10. [[CrossRef](#)]
26. Jin, D.; Ruan, J.; Li, S.; Meng, B.; Wang, L. Modelling and validation of a roller-cam rail mechanism used in a 2D piston pump. *J. Zhejiang Univ. Sci. A* **2019**, *20*, 201–217. [[CrossRef](#)]
27. Guilan, T.; Haibo, F.; Weiyi, Z. A New Method of Torque Compensation for High Speed Indexing Cam Mechanism. *J. Mech. Des.* **1999**, *121*, 319–323. [[CrossRef](#)]
28. Ambardekar, M.N.; Gupta, K.N. Stochastic Optimal Control of Vibrations of a High-Speed Cam-Driven Mechanism. *Mech. Mach. Theory* **1990**, *25*, 59–68. [[CrossRef](#)]
29. Hsu, W.; Pisano, A.P. Modeling of a Finger-Follower Cam System with Verification in Contact Forces. *J. Mech. Des.* **1996**, *118*, 132–137. [[CrossRef](#)]
30. Liu, H.-T.J. Synthesis and Steady-State Analysis of High-Speed Elastic Cam-Actuated Linkages with Fluctuated Speeds by a Finite Element Method. *J. Mech. Des.* **1997**, *119*, 395–402. [[CrossRef](#)]
31. Dresner, T.L.; Barkan, P. New Methods for the Dynamic Analysis of Flexible Single-Input and Multi-Input Cam-Follower Systems. *J. Mech. Des.* **1995**, *117*, 150–155. [[CrossRef](#)]
32. Wang, Y.; Wang, Z. Dynamic Analysis of Flexible Mechanisms with Clearances. *J. Mech. Des.* **1996**, *118*, 592–594. [[CrossRef](#)]
33. Paradorn, V. An Impact Model for the Industrial Cam-Follower System: Simulation and Experiment. Master's Thesis, Worcester Polytechnic Institute, Worcester, MA, USA, October 2007.
34. Kuang, J.-H.; Hsu, C.-M.; Hu, C.-C. Dynamic behavior of globoidal cam systems with torque compensation mechanisms. *Mech. Mach. Theory* **2010**, *45*, 1201–1214. [[CrossRef](#)]

35. Desai, H.D.; Patel, V.K. Computer Aided Kinematic and Dynamic Analysis of Cam and Follower. In Proceedings of the WCE 2010, London, UK, 30 June–2 July 2010.
36. Zhang, Y.; Li, R.; Xiao, L.; Yang, J. Study on Dynamic Simulation of Cam Mechanism Based on Pro/E and ADAMS. In Proceedings of the 2nd International Conference on Electronic & Mechanical Engineering and Information Technology, Shenyang, China, 7 September 2012; Atlantis Press: Paris, France, 2012; pp. 1229–1232.
37. Delyová, I.; Hroncová, D.; Sivák, P.; Beliško, M. The Dynamic Analysis of Cam Mechanism. *Am. J. Mech. Eng.* **2013**, *1*, 266–270.
38. Jomartov, A. Multibody Dynamic Model of Russian Sulzer Loom STB. *J. Vibr. Eng. Technol.* **2017**, *5*, 523–533.
39. Deng, Y.; Zhang, J.; Zhu, T.; Duan, T. Dynamic analysis of high speed cam linkage mechanism of chocolate packaging machine. *Acad. J. Manuf. Eng.* **2020**, *18*, 79–84.
40. Jiang, Z.; Zhu, T.; Chen, Z.; Fan, R.; Gao, Y.; Zhang, H.; Wang, L. A General Design Method of Cam Profile Based on Cubic Splines and Dynamic Model: Case Study of a Gravity-Driven Tricycle. *Mathematics* **2022**, *10*, 1979. [[CrossRef](#)]
41. Vo, N.Y.P.; Le, T.D. Dynamic Analysis of Quasi-Zero Stiffness Pneumatic Vibration Isolator. *Appl. Sci.* **2022**, *12*, 2378. [[CrossRef](#)]
42. Osman, M.O.M.; Bahgat, B.M.; Osman, M. Dynamic Analysis of a Cam Mechanism with Bearing Clearances. *Mech. Mach. Theory* **1987**, *22*, 303–314. [[CrossRef](#)]
43. Chang, X.; Pan, H.; Xu, J.; Wang, T. Study of Fault Identification of Clearance in Cam Mechanism. *Appl. Sci.* **2022**, *12*, 7420. [[CrossRef](#)]
44. Rao, A.C. Minimum Flexibility Error and Optimum Sensitivity Synthesis of Cam Mechanisms. *Mech. Mach. Theory* **1979**, *14*, 209–214. [[CrossRef](#)]
45. Lassaad, W.; Mohamed, T.; Yassine, D.; Fakher, C.; Taher, F.; Mohamed, H. Nonlinear dynamic behaviour of a cam mechanism with oscillating roller follower in presence of profile error. *Front. Mech. Eng.* **2013**, *8*, 127–136. [[CrossRef](#)]
46. De Groote, W.; Van Hoecke, S.; Crevecoeur, G. Physics-Based Neural Network Models for Prediction of Cam-Follower Dynamics Beyond Nominal Operations. *IEEE/ASME Trans. Mechatron.* **2022**, *27*, 2345–2355. [[CrossRef](#)]
47. Lin, T.-C.; Schabacker, M.; Ho, Y.-L.; Kuo, T.-C.; Tsay, D.-M. Geometric Design and Dynamic Analysis of a Compact Cam Reducer. *Machines* **2022**, *10*, 955. [[CrossRef](#)]
48. Flocker, F. Addressing Cam Wear and Follower Jump in Single-Dwell Cam-Follower Systems with an Adjustable Modified Trapezoidal Acceleration Cam Profile. *J. Eng. Gas Turbines Power* **2009**, *131*, 032804. [[CrossRef](#)]
49. Podgornyj, Y.I.; Skeebe, V.Y.; Martynova, T.G.; Pechorkina, N.S.; Skeebe, P.Y. Kinematic analysis of crank-cam mechanism of process equipment. *IOP Conf. Ser. Mater. Sci. Eng.* **2018**, *327*, 042080. [[CrossRef](#)]
50. Merticaru, V.; Merticaru, E. About Two Different Dynamically Modeling Approaches for a Cam Mechanism from an Automate Feeding System. In *Annals of the Oradea University: Fascicle Management and Technological Engineering*; Oradea University: Oradea, Romania, 2009; Volume VIII (XVIII), pp. 373–380.
51. Johnson, K. *Contact Mechanics*; Cambridge University Press: Cambridge, UK, 1985; pp. 84–406. [[CrossRef](#)]
52. Synthesis of Cam Mechanisms. Available online: <http://www.mec.upt.ro/fisiere/mecanisme/05%20Sinteza%20mecanismelor%20cu%20came.pdf> (accessed on 31 May 2023). (In Romanian)

Disclaimer/Publisher’s Note: The statements, opinions and data contained in all publications are solely those of the individual author(s) and contributor(s) and not of MDPI and/or the editor(s). MDPI and/or the editor(s) disclaim responsibility for any injury to people or property resulting from any ideas, methods, instructions or products referred to in the content.